Final Report

(December 9, 2004 – December 31, 2009)

Project Title: Effects and Mechanisms of Mechanical Activation on Hydrogen Sorption/ Desorption of Nanoscale Lithium Nitrides

Project Period: December 9, 2004 – December 31, 2009
Date of Report: December 31, 2009

Recipient: University of Connecticut
Award Number: DE-FC36-05GO15008

Project Director/Principal Investigator: Leon L. Shaw (UConn)
Co-Principal Investigator: Z. Gary Yang (PNNL)
Team Members: Kyle Crosby (UConn), Xuefei Wan (UConn), Yang Zhong (UConn), Tippawan Markmaitree (UConn, currently at URI), William Osborn (UConn, currently at NIST), Jianzhi Hu (PNNL), Ja Hun Kwak (PNNL)

Cost-Sharing Partners: University of Connecticut (UConn)

Contact: Leon L. Shaw, (860) 486-2592 (Tel), Leon.Shaw@Uconn.Edu; Department of Chemical, Materials and Biomolecular Engineering, University of Connecticut, Storrs, CT 06269

DOE Managers: DOE HQ Technology Manager: Ned T. Stetson
DOE Field Project Officer: Katie Randolph

Executive Summary

The objective of this project is to investigate and develop novel, mechanically activated, nanoscale Li_3N-based and $LiBH_4$-based materials that are able to store and release ~10 wt% hydrogen at temperatures near 100°C with a plateau hydrogen pressure of less than 10 bar. Four (4) material systems have been investigated in the course of this project in order to achieve the project objective. These 4 systems are (i) $LiNH_2$+LiH, (ii) $LiNH_2$+MgH_2, (iii) $LiBH_4$, and (iv) $LiBH_4$+MgH_2. The key findings we have obtained from these 4 systems are summarized below.

- The thermodynamic driving forces for $LiNH_2$+LiH and $LiBH_4$ systems are not adequate to enable H_2 release at temperatures < 100°C.
- Hydrogen release in the solid state for all of the four systems is controlled by diffusion, and thus is a slow process.
- $LiNH_2$+MgH_2 and $LiBH_4$+MgH_2 systems, although possessing proper thermodynamic driving forces to allow for H_2 release at temperatures < 100°C, have sluggish reaction kinetics because of their diffusion-controlled rate-limiting steps.

- Reducing particles to the nanometer length scale (< 50 nm) can improve the thermodynamic driving force to enable H_2 release at near ambient temperature, while simultaneously enhancing the reaction kinetics as well as changing the diffusion-controlled rate-limiting step to gas desorption-controlled rate-limiting step. This phenomenon has been demonstrated with $LiBH_4$ and offers the hope that further work along this direction will make one of the material systems, i.e., $LiBH_4$, $LiBH_4$+MgH_2 and $LiNH_2$+MgH_2, possess the desired thermodynamic properties and rapid H_2 uptake/release kinetics for on-board applications.

Many of the findings and knowledge gained from this project have been published in archival refereed journal articles [1-15] and are accessible by general public. Thus, to avoid a bulky final report, the key findings and knowledge gained from this project will be succinctly summarized, particularly for those findings and knowledge available in the public domain. However, for those findings and knowledge that have not been published yet, more detailed information will be provided. The report will be divided into 4 major sections based on the material systems investigated.

Section I: $LiNH_2$ + LiH System

1.1 The reaction pathway for dehydriding of the $LiNH_2$+LiH system: The dehydrogenation reaction of the $LiNH_2$ + LiH system can be described as [1]

$$LiNH_2 + LiH \Rightarrow Li_2NH + H_2 \quad (1)$$

Although Reaction (1) is a reaction between two solids, it is actually mediated by a gaseous phase because Reaction (1) proceeds with two elementary reactions, as shown below [2-4].

$$LiNH_2 \Rightarrow \tfrac{1}{2}\, Li_2NH + \tfrac{1}{2}\, NH_3 \quad (2)$$
$$\tfrac{1}{2}\, NH_3 + \tfrac{1}{2}\, LiH \Rightarrow \tfrac{1}{2}\, LiNH_2 + \tfrac{1}{2}\, H_2 \quad (3)$$

The involvement of NH_3 in the dehydrogenation process is the reason why many investigators find NH_3 emission from the $LiNH_2$ + LiH system [3-6].

1.2 The rate-limiting step for dehydriding of the $LiNH_2$+LiH system: The dehydrogenation process of the $LiNH_2$ + LiH system is controlled by diffusion [2]. Reaction (3) takes place very fast on the order of microseconds because the solid product $LiNH_2$ spalls off from the surface of the solid reactant LiH. In contrast, Reaction (2) is diffusion controlled because the solid product Li_2NH forms a shell on the surface of the solid reactant $LiNH_2$ [2]. As a result, the gaseous product NH_3 has to diffuse through the Li_2NH shell in order for Reaction (2) to continuously take place [2,7]. This understanding has far-reaching implications because nearly all of the reversible hydrogen storage systems are involved with gas-solid or solid-solid reactions, many of which are likely to be diffusion controlled. If a reaction is diffusion controlled, then effective methods can be taken to enhance the reaction kinetics. These effective methods can include:

- nanoengineering to reduce the diffusion distance,
- increasing the composition gradient for diffusion via advanced catalysts,

- increasing the diffusion coefficient via doping to introduce internal strains and vacancies, and
- micro-alloying to induce spallation of the reaction product layer or extensive cracking so that diffusion will no longer be a rate-controlling step.

1.3 The mechanism for the fast hydriding rate of the $LiNH_2$ + LiH system: The overall reaction for the hydriding process can be written as

$$Li_2NH + H_2 \Rightarrow LiNH_2 + LiH \qquad (4)$$

This reaction is very fast because it is not controlled by the diffusion process [8]. The reaction products $LiNH_2$ and LiH form a cracked layer outside the Li_2NH core, but not spalling off. As a result, H_2 is readily available to react with Li_2NH even at temperatures as low as 200°C [8]. In contrast, for the dehydriding process, a reaction controlled by diffusion, to proceed with noticeable rates, temperatures as high as 285°C are needed. This understanding underscores the importance in selecting the hydrogen storage materials with non-diffusion controlled reactions or converting the diffusion-controlled to non-diffusion controlled reactions through various methods listed in Section 1.3.

1.4 The effect of mechanical activation on the characteristics of the $LiNH_2$ + LiH system: High-energy ball milling leads to finer particle sizes, large surface areas, high defect densities, smaller crystallites, and intimate mixing of reactants at nanoscales [3,7-11]. However, the particles produced from high-energy ball milling are typically nanostructured with submicrometer sizes and nanocrystalline grains. Furthermore, a size distribution of nanocrystalline grains is normally present, and the crystallite size distribution becomes narrower as the ball milling time increases [11]. Ball milling at liquid nitrogen temperature can further increase the defect density in nanocrystalline particles [12]. All of these changes to the powder characteristics have substantial impacts on the hydriding and dehydriding properties of mechanically activated particles. Specifically, increasing the degree of mechanical activation results in (i) a decrease in the activation energy of the dehydriding process, (ii) a decrease in the dehydriding temperature, and (iii) a higher dehydriding rate [3,4,10,12,13].

1.5 The effect of mechanical activation on the hydriding and dehydriding properties of the $LiNH_2$ + LiH system: The refinement of crystallite and particle sizes, the increase in the surface area and defect concentrations, and intimate mixing of reactants can drastically enhance the hydriding and dehydriding kinetics. Specifically, through mechanical activation, we have demonstrated the highest enhancement of $LiNH_2$ to Li_2NH transition (i.e., reducing the onset temperature for the $LiNH_2$ to Li_2NH transition from 120°C to room temperature [7], the lowest hydriding and dehydriding temperatures for the $LiNH_2$ + LiH system (e.g., the onset temperature for releasing hydrogen is reduced to near room temperature) [3], and the hydrogen release from the $LiNH_2$ + LiH system with NH_3 emission below the detection limit of the mass spectroscopy [3]. All of these improvements are substantial, but not sufficient for real world applications where H_2 release and uptake at temperatures < 100°C are needed. Further improvements would require additional reduction in the particle size since (i) all of the reactions investigated are controlled by diffusion and (ii) ball milling only reduces the

particle size to the submicrometer scale. In contrast, nanometer particles (as we observed in pure $LiBH_4$, Section III) have the potential to alter the rate-limiting step from the diffusion controlled reaction to non-diffusion-controlled reaction, thereby greatly enhancing the reaction kinetics.

1.6 The cyclic stability of the mechanically activated $LiNH_2$ and LiH system: The mechanically activated $LiNH_2$ + LiH system is unusually stable over the course of 60 hydriding and dehydriding cycles at 285°C for more than 200 hours [8,13]. Note that 285°C is equivalent to 86% of $LiNH_2$'s melting temperature and 58% of LiH's melting temperature. At such high homologous temperatures, most materials will be fully densified. However, after exposure to such high homologous temperatures for more than 200 hours, $LiNH_2$ and LiH grains remain to be at the nanoscale [8,13]. The unusual cyclic stability has been attributed to the low green density of mechanically activated powder compacts, which provides the high resistance against grain growth and decrease in the specific surface area [8]. Phase transformation induced by hydriding and dehydriding reactions has a minor effect on stabilizing the grain size and specific surface area, as does the effect of two-phase compacts in comparison to the effect of the green packing density [8]. This understanding underscores the importance of preparing a uniform and loosely packed powder aggregate through proper high-energy ball milling conditions.

Section II: $LiNH_2$ + MgH_2 System

2.1 Reaction pathway for dehydrogenation of the $2LiNH_2$ + MgH_2 system: The overall dehydrogenation reaction for the $2LiNH_2$ + MgH_2 system, as shown in Eq. (5), has been identified as follows [14].

$$2\ LiNH_2 + MgH_2 \rightarrow Li_2Mg(NH)_2 + 2\ H_2 \quad (5)$$

First, $2LiNH_2$ decomposes, as shown below.

$$2\ LiNH_2 \Rightarrow Li_2NH + NH_3 \quad (6)$$

Then the NH_3 from Reaction (6) reacts with MgH_2 to form $Mg(NH_2)_2$ and H_2:

$$NH_3 + ½\ MgH_2 \Rightarrow ½\ Mg(NH_2)_2 + H_2 \quad (7)$$

The ½ $Mg(NH_2)_2$ from Reaction (7) decomposes to form ½ MgNH and ½ NH_3:

$$½\ Mg(NH_2)_2 \Rightarrow ½\ MgNH + ½\ NH_3 \quad (8)$$

The ½ NH_3 formed from Reaction (8) reacts again with the un-reacted MgH_2 according to Reaction (7), and the $Mg(NH_2)_2$ formed decomposes again according to Reaction (8) to form MgNH and NH_3. Such a reaction cycle continues according to Reactions (7) and (8) until all MgH_2 has reacted with NH_3. The products from this reaction cycle are H_2 and MgNH. The MgNH formed reacts with the Li_2NH from Reaction (6) to form $Li_2MgN_2H_2$, as defined by Reaction (9).

$$MgNH + Li_2NH \Rightarrow Li_2MgN_2H_2 \quad (9)$$

Thus, although Reaction (5) is a reaction between two solids, it is actually mediated by NH_3. The reaction rate of NH_3 with MgH_2 is, therefore, critical in determining the dehydrogenation rate of the $2LiNH_2+MgH_2$ system and whether there is NH_3 emission from the $2LiNH_2 + MgH_2$ system.

2.2 The reaction rate of NH_3 with MgH_2 and LiH: The reaction between MgH_2 and NH_3 is very slow. It is slower than the reaction between LiH and NH_3 on the basis of per hydride surface area, per the reaction volume of the hydride, and per the number of moles of the hydride [15]. Therefore, to minimize the problem of NH_3 emission from $LiNH_2$-containing systems, the use of MgH_2 should be avoided, while LiH should be utilized. Based on this guideline, one way to utilize the favorable thermodynamic properties of Reaction (5) while avoiding the NH_3 emission problem is to start with $Mg(NH_2)_2$ rather than MgH_2, as shown below.

$$Mg(NH_2)_2 + 2\ LiH \Longleftrightarrow Li_2Mg(NH)_2 + 2\ H_2 \quad (10)$$

The dehydrogenation rate of Reaction (10) is very fast, as shown in Fig. 1. However, the precise reason why the dehydrogenation rate of Reaction (10) is fast has not been investigated yet.

2.3 The reaction rate of $LiNH_2$ with MgH_2 to form $Li_2Mg(NH)_2$: The H_2 release rate from the $2LiNH_2+MgH_2$ mixture, as shown by Reaction (5), is faster than the $LiNH_2$+LiH mixture at 210^oC because of the higher thermodynamic driving force of the $2LiNH_2+MgH_2$ system [14]. However, the $2LiNH_2+MgH_2$ mixture has a lower rate in reaching its equilibrium gas pressure than the $LiNH_2$+LiH mixture [14]. These results indicate that the $2LiNH_2+MgH_2$ mixture has a higher thermodynamic driving force, but lower reaction kinetics than the $LiNH_2$+LiH mixture. The reaction kinetics of the $2LiNH_2+MgH_2$ mixture is so sluggish that a total of 70 h at 240°C with multiple holding and evacuation sub-steps (100 sub-steps) is required to achieve the complete conversion from $2LiNH_2+MgH_2$ to $Li_2Mg(NH)_2$ [16]. Furthermore, the same holding time (70 h) at 210°C with the same number of the evacuation sub-steps (100 sub-steps) does not lead to the complete conversion [16].

2.4 The hydriding kinetics and rate-limiting step of $Li_2Mg(NH)_2$: The hydriding process of $Li_2Mg(NH)_2$ is very sluggish even though it has favorable thermodynamic properties for near the ambient temperature operation. Holding at 200°C for 10 h only results in 3.75 wt% H_2 uptake. This is clearly not sufficient for on-board applications. It is found that the rate-limiting step for the hydriding process of $Li_2Mg(NH)_2$ is diffusion [16]. Thus, the future direction to enhance the hydriding kinetics of $Li_2Mg(NH)_2$–based hydrogen storage material system should entail: (i) nano-engineering to minimize the diffusion distance, (ii) high-energy ball milling to introduce lattice defects and thus increase the diffusion coefficient, and/or (iii) doping to increase the lattice distortion and thus the diffusion rate.

Section III: $LiBH_4$ System

3.1 Dehydrogenation characteristics of nanoscale $LiBH_4$: Pure nanoscale $LiBH_4$ powders synthesized from a $LiBH_4$ in a tetrahydrofuran (THF) solution (termed as the $LiBH_4$/THF solution hereafter) can release much more H_2 than the micrometer-sized $LiBH_4$ powder (see Fig. 2) [7]. As shown in Fig. 2, the nanoscale $LiBH_4$ powder can release 3.5 wt% H_2 from 25 to 265°C. If partially oxidized, the amount of H_2 released from the nanoscale $LiBH_4$ will be reduced. Nevertheless, the amounts of H_2 released from both nanoscale $LiBH_4$ powders shown in Fig. 2 are clearly higher than any previously reported numbers for pure bulk $LiBH_4$ powder [18-22]. The typical number for pure bulk $LiBH_4$ powder reported in the open literature is ~0.5 wt% H_2 from 25 to 265°C [18-22]. We note that the previously reported numbers [18-22] are obtained from continuous heating, rather than heating and then holding at 265°C as shown here. Thus, we have subjected bulk $LiBH_4$ powder at the as-purchased condition to dehydrogenation with the same heating and holding condition as the nanoscale $LiBH_4$ powder. As shown in Fig. 2, the amount of H_2 released from the bulk $LiBH_4$ powder is 0.75 wt% after holding at 265°C for 5 h. This number is slightly larger than 0.5 wt% reported in the literature [18-22] because of the 5-h additional holding at 265°C. The improvement of the nanoscale $LiBH_4$ over the bulk $LiBH_4$ in releasing H_2 observed in this study is about four folds, and is attributed to the formation of nanoparticles when $LiBH_4$ is derived from the $LiBH_4$/THF solution, as will be discussed later.

Figure 2 also reveals that both nanoscale $LiBH_4$ powders display an onset temperature for hydrogen release (< 0.1% H_2) at ~35°C. This temperature is the lowest onset temperature ever reported for releasing H_2 from $LiBH_4$. Previously, the onset temperature that can lead to release of approximately 1 wt% H_2 or more is reported to be ~150°C when $LiBH_4$ particles of ~5 nm are embedded in mesoporous carbon [23] and ~220°C when $LiBH_4$ particles of ~3 nm is confined within activated carbon [24]. For bulk $LiBH_4$ powder, the corresponding onset temperature is at or higher than the melting temperature of $LiBH_4$ (280°C) [18-22].

3.2 Effluent gas from nanoscale $LiBH_4$: To confirm the gas released from the nanoscale $LiBH_4$ is indeed H_2, the dehydriding behavior of the nanoscale $LiBH_4$ powder was also investigated using thermogravimetric analysis (TGA) in conjunction with an on-line residual gas analyzer (RGA). One such result is shown in Fig. 3. As shown, the nanoscale $LiBH_4$ powder exhibits weight gain rather than the expected weight loss. This unexpected behavior is due to the extreme reactivity of the nanoscale $LiBH_4$ powder. This powder is so reactive that it gets oxidized under a flowing argon atmosphere containing a small amount of residual oxygen from air, leading to weight gain rather than weight loss. Note that such a weight gain event even occurs at room temperature before heating, indicating the extreme reactivity of the nanoscale $LiBH_4$ powder. In spite of the complication from oxidation, the RGA data clearly reveals several interesting phenomena. First, there is no THF release during the entire heating process, i.e., the THF solvent has been completely removed from the nanoscale $LiBH_4$ powder before the TGA/RGA study. Second, there is no borane (B_2H_6) release during heating. The only gas released is H_2. Therefore, it can be concluded that the quantity of the hydrogen determined from the pressure-composition-temperature (PCT) device (Fig. 2) is accurate. The absence of borane – an impurity that is likely to poison polymer electrolyte membrane (PEM) fuel cells and frequently found in the hydrogen released from $LiBH_4$ [22], suggests that emission of borane can be avoided if hydrogen is released at low temperatures.

Other important phenomena in Fig. 3 include the following. (a) Temporary weight loss is observed whenever there is a large release of H_2. This phenomenon is due to the formation of a H_2 gas blanket over the nanoscale $LiBH_4$ powder, which prevents the oxidation of the powder. The onset temperatures for the first, second and third weight loss events are ~50°C, ~225°C and ~280°C, respectively. Note that during these temporary weight loss events there is no emission of borane and THF, reinforcing the conclusion that H_2 is the only gas released from the nanoscale $LiBH_4$. (b) The two largest sudden increases in the hydrogen intensity occur at ~50°C and ~280°C, suggesting that most of the hydrogen stored in $LiBH_4$ is released at these two temperature ranges. (c) Most of the H_2 stored in the nanoscale $LiBH_4$ is released below 350°C. This is a dramatic improvement over bulk $LiBH_4$ powder which releases most of its hydrogen at temperatures from 400°C to 680°C [18-21,25,26].

3.3 Reversibility of nanoscale $LiBH_4$: Figure 4 shows the dehydriding and re-hydriding behavior of the nano-$LiBH_4$ powder. Note that in this dehydriding and re-hydriding cyclic experiment, the first segment of the cycle is dehydrogenation. In addition, we note that the starting point for re-hydrogenation is not at the origin of the coordinate, but at approximately 1 wt% H_2. Our careful calibration reveals that the hydrogen uptake of 1 wt% at room temperature shown in Figure 4 is the artifact of the PCT device induced by the "dead volume" in valves. Thus, the quantity of the hydrogen uptake shown in Figure 4 should be subtracted by 1 wt%. Armed with this information, we can state that the first dehydrogenation after holding at 265°C for 5 h results in release of 3.5 wt% H_2 from the nano-$LiBH_4$ powder, whereas the first re-hydrogenation only takes up about 1.7 wt% H_2, indicating that the hydrogen release and uptake capacity are not completely reversible at the testing condition investigated.

Figure 4 also reveals that the second dehydrogenation only releases ~1.85 wt% H_2, which is roughly 50% of the hydrogen released in the first dehydrogenation and approximately equal to the amount of H_2 taken up in the first re-hydrogenation. It is interesting to note that the second re-hydrogenation and the third dehydrogenation all exhibit ~1.85 wt% H_2 uptake and release, respectively, suggesting that the hydrogen uptake and release capacity may stabilize at about 1.85 wt% H_2 at the testing condition imposed. These results indicate that the hydrogen uptake and release capacity of the nano-$LiBH_4$ powder is only partially reversible, which is in good agreement with the previous studies of nano-$LiBH_4$ confined within activated carbon [24] and embedded in mesoporous carbon [23]. However, it should be stressed that even with the partial reversibility, the re-hydrogenation properties exhibited by the nano-$LiBH_4$ powder are much better than that of bulk $LiBH_4$ which displays practically no hydrogen uptake at temperatures below 450°C [21].

3.4 TEM analysis of nanoscale $LiBH_4$: In order to understand why the $LiBH_4$ powder derived from the $LiBH_4$/THF solution has much better dehydriding and re-hydriding properties than bulk $LiBH_4$ [18-21,25,26], the nanoscale $LiBH_4$ powder has been characterized using transmission electron microscopy (TEM). Fig. 5 shows TEM images and selected area diffraction (SAD) patterns of the pure $LiBH_4$ powder derived from the $LiBH_4$/THF solution. The SAD pattern shows that the pure $LiBH_4$ powder is an amorphous phase, and thus the contrast in the bright-field images is due to the thickness variation rather than the diffraction contrast. Note that the $LiBH_4$ powder derived from the $LiBH_4$/THF solution can take on

several morphologies such as chucks, thin films and particles. In spite of its multiple morphologies, the $LiBH_4$ powder is actually aggregates composed of ultrafine particles or films with basic units of irregular shapes and sizes ranging from 20 to 50 nm. These aggregates and films contain extensive pores which separate ultrafine particles and the basic units of irregular shapes. These nanopores provide rapid channels for the H_2 gas to move in and out so that an aggregate of a few micrometers (e.g., Fig. 5a) can have thermodynamic and kinetic properties like nanoparticles of 20 to 50 nm. In short, the TEM analysis unambiguously unveils that the pure $LiBH_4$ powder derived from the $LiBH_4$/THF solution can be described as aggregates of amorphous nanoscale particles of 20 to 50 nm.

3.5 FTIR analysis of nanoscale $LiBH_4$: The chemical nature of the nanoscale $LiBH_4$ attained from the $LiBH_4$/THF solution has been assessed using Fourier transform infrared (FTIR) spectroscopy. Figure 6 shows the FTIR spectrum of the nanoscale $LiBH_4$ powder with the second stage of drying being carried out in the PCT chamber in comparison with those of the as-purchased bulk $LiBH_4$ powder, the as-purchased $LiBO_2$ powder, and water. It is noted that the as-purchased bulk $LiBH_4$ powder matches the characteristic absorption frequencies (2384, 2291, 2225, and 1126 cm^{-1}) of $LiBH_4$ identified previously [26,27]. However, it also contains moisture. The nanoscale $LiBH_4$ derived from the $LiBH_4$/THF solution manifests the same FTIR spectrum as the bulk $LiBH_4$ except several small absorption peaks present between 900 and 1400 cm^{-1}. These small peaks are not due to THF because no THF is detected during the TGA/RGA analysis, as discussed previously (Fig. 3). These small peaks are also unlikely to be indicative of THF/$LiBH_4$ solvates because no shifting of the characteristic absorption peaks of $LiBH_4$ is observed. Another possible chemical species that may cause these small peaks is $LiBO_2$ resulting from the possible oxidation of some nanoscale $LiBH_4$. However, as shown in Fig. 6b, none of these small peaks can match the characteristic absorption peaks of the commercially available $LiBO_2$ powder, ruling out the possibility of the presence of $LiBO_2$ in the nanoscale $LiBH_4$ powder. The possibility of the presence of hydrated $LiBO_2$ has also been considered. However, FTIR studies of hydrated $LiBO_2$ (see Supporting Information) reveal that the small peaks present between 900 and 1400 cm^{-1} in the nanoscale $LiBH_4$ powder cannot be accounted for by hydrated $LiBO_2$. As a result, the source of these small absorption peaks remains unidentified at this stage. Nevertheless, the FTIR analysis unveils that the nanoscale powder derived from the $LiBH_4$/THF solution is predominately $LiBH_4$.

Figure 7 shows how the FTIR spectrum of the nanoscale $LiBH_4$ powder changes with dehydrogenation and re-hydrogenation treatments at 265^oC. Note that after one dehydrogenation treatment at 265^oC (R1) the sample still contains the characteristic absorption frequencies of $LiBH_4$. This data is in good accordance with the fact that only 3.4 wt% H_2 is released in the dehydrogenation process (Fig. 2). The nanoscale $LiBH_4$ powder after two dehydrogenation and re-hydrogenation cycles at 265^oC (i.e., 2(R+S)) also exhibits the characteristic absorption frequencies of $LiBH_4$. This is consistent with the expectation because only a part of the nanoscale $LiBH_4$ has participated in dehydrogenation and re-hydrogenation at 265^oC. It is also noted that those small unidentified absorption peaks have undergone some changes in the dehydrogenation and re-hydrogenation process. The nature of these changes, however, cannot be defined at this stage. Additional studies are needed in the future to resolve this issue.

The most interesting phenomenon in dehydrogenation and re-hydrogenation of the nanoscale $LiBH_4$ at 265°C is the formation of $Li_2B_{12}H_{12}$ because the characteristic B-H stretching vibration from $Li_2B_{12}H_{12}$ at 2479 cm^{-1} [28] is present for both R1 and 2(R+S) samples. Furthermore, the intensity of this absorption peak increases with the number of the release treatment. The B-B absorption from $Li_2B_{12}H_{12}$ at 1070 cm^{-1} [28], however, is not discernable because of its intrinsically low intensity and overlap with the unidentified small peaks at that region. Nevertheless, the appearance of the 2479 cm^{-1} peak in both R1 and 2(R+S) samples reveals that $Li_2B_{12}H_{12}$ can be formed at 265°C or lower from the nanoscale $LiBH_4$ powder. This formation temperature is about 160°C lower than that reported previously for bulk $LiBH_4$ (427 – 457°C) [29].

3.6 Enhancements in hydrogen storage properties via thermodynamic and kinetic effects: The improved hydrogen storage properties of the nanoscale $LiBH_4$ shown in Fig. 2 are enhanced by thermodynamic and kinetic effects. As shown in Fig. 8, the dissociation pressure of the nanoscale $LiBH_4$ is ~1.37 bar at 265°C, which is ~270% higher than the dissociation pressure of the bulk $LiBH_4$ (~0.37 bar) measured under the same dehydrogenation condition. Figure 8 unequivocally indicates that the dissociation pressure of the nanoscale $LiBH_4$ is approximately 270% higher than that of the bulk counterpart. This increased dissociation pressure is likely the reason why the nanoscale $LiBH_4$ can release H_2 at ~35°C, and it may also be the key factor for the formation of $Li_2B_{12}H_{12}$ at 265°C or lower.

The kinetic effect of the nanoscale $LiBH_4$ can be appreciated by close examination of Fig. 2 where the hydrogen release is conducted at isothermal (265°C) and isobaric (0.01 bar) conditions when the time is larger than 2.2 h. Through curve fitting of the isothermal dehydrogenation section (i.e., for time > 2.2 h), we find that dehydrogenation of the nanoscale $LiBH_4$ is controlled by gas desorption at the surface of $LiBH_4$ particles, whereas dehydrogenation of the bulk $LiBH_4$ is controlled by diffusion. As shown in Fig. 9, the dehydrogenation data of the bulk $LiBH_4$ at 265°C fits well the diffusion-controlled reaction of a core-shell model [27] with the following fitting equation

$$(1 - f)^{1/3} = 1.7178 - 0.008t^{1/2} \quad \text{and} \quad R^2 = 0.93 \qquad (11)$$

where f is the fraction reacted and t is the reaction time. In contrast, the nanoscale $LiBH_4$ (i.e., curve *b* in Fig. 2) exhibits a very poor fit with the diffusion-controlled reaction, but a good fit with a gas desorption model [27], as shown in Fig. 10. The fitting equation is found to be

$$f = -0.425 + 6\text{x}10^{-5}\, t \quad \text{and} \quad R^2 = 0.99 \qquad (12)$$

Curve *a* of the nanoscale $LiBH_4$ in Fig. 2 also displays a good fit with the gas desorption-controlled model (not shown here). Therefore, the nanoscale $LiBH_4$ has altered the rate-limiting step for dehydrogenation from the diffusion-controlled to gas desorption-controlled reaction.

In addition to changing rate-limiting step, the nanoscale $LiBH_4$ has increased the hydrogen release rate substantially. At the time of 2.5 h in Fig. 2, the hydrogen release rate of the nanoscale $LiBH_4$ without oxidation is 0.392 wt% per hour, which is about 45% higher than the hydrogen release rate of the bulk $LiBH_4$. At the time of 6.0 h, the difference between

them increases further, that is, the hydrogen release rate of the bulk $LiBH_4$ drops to 0.054 wt% per hour, whereas the hydrogen release rate of the nanoscale $LiBH_4$ remains to be 0.392 wt% per hour, representing more than 500% higher than the hydrogen release rate of the bulk $LiBH_4$.

3.7 Summary for the $LiBH_4$ system: The nanoscale $LiBH_4$ powder synthesized via a solvent evaporation process takes on multiple morphologies and can be described as aggregates of amorphous nanoscale particles of 20 to 50 nm. The nanoscale $LiBH_4$ exhibits many novel properties, including the ultralow onset temperature for releasing H_2 (at 35°C), very large quantities of H_2 release and uptake in the solid state, and formation of $Li_2B_{12}H_{12}$ at 265°C or lower. These novel properties are associated with improvements in both the thermodynamic driving force and reaction kinetics. The dissociation pressure of the nanoscale $LiBH_4$ in the solid state at 265°C is ~270% higher than that of the bulk counterpart. Nanoscale $LiBH_4$ not only enhances the dehydrogenation kinetics by 45 to 500%, but also alters the rate-limiting step from the diffusion-controlled to gas desorption-controlled reaction. These results demonstrate that nano-engineering can be a very effective approach to attain novel properties that are not available from bulk $LiBH_4$.

Section IV: $LiBH_4 + MgH_2$ System

4.1 The behavior of solid-state hydrogenation of $2LiH + MgB_2$ to form $LiBH_4 + MgH_2$: The overall reversible reaction for the $LiBH_4 + MgH_2$ system has been proposed to be [26]

$$2LiBH_4 + MgH_2 \Longleftrightarrow 2LiH + MgB_2 + 4H_2 \qquad (13)$$

It is found that the solid-state hydriding reaction of the $2LiH+MgB_2$ mixture is diffusion controlled [27]. Such diffusion-controlled hydrogenation can be enhanced greatly by high-energy ball milling. Through effective ball milling we have demonstrated, for the first time, that 8.3 wt.% hydrogen uptake can be obtained from the $LiH + MgB_2$ system in the solid state without any catalysts. The attainment of solid-state hydrogenation with appreciable hydrogen uptake is attributed to nano-engineering and mechanical activation. The smaller grain size and higher lattice microstrain induced by high-energy ball milling lead to faster diffusion rates and thus faster hydrogenation rates [27].

4.2 Reaction pathway for solid-state hydrogenation of $LiH + MgB_2$ to form $LiBH_4 + MgH_2$: The overall reversible reaction for the $LiBH_4 + MgH_2$ system is shown in Reaction (13). However, the solid-state hydrogenation of $2LiH+MgB_2$ has been identified to proceed in two elementary steps as shown below [30-32].

$$2LiH + MgB_2 \Rightarrow (Mg_{1-x}Li_{2x})B_2 + xMgH_2 + (2-2x)LiH \qquad (14)$$

$$(Mg_{1-x}Li_{2x})B_2 + (2-2x)LiH + 4H_2 \Rightarrow 2LiBH_4 + MgH_2 \qquad (15)$$

The first step is the ion exchange between Mg and Li ions within MgB_2 to form an intermediate compound, $(Mg_{1-x}Li_{2x})B_2$, and the second step is the continuous Mg-Li ion exchange and simultaneous hydrogenation of the intermediate compound, $(Mg_{1-x}Li_{2x})B_2$, to

form the final product $LiBH_4$. Both elementary steps require the outward diffusion of Mg ions and the inward diffusion of Li ions within $(Mg_{1-x}Li_{2x})B_2$ compound. The inward diffusion of H is also necessary for the second step. This reaction pathway is consistent with the observed diffusion-controlled hydriding kinetics [27].

4.3 The behavior of solid-state dehydrogenation of the $2LiBH_4+MgH_2$ mixture: The dehydrogenation behavior of the $2LiBH_4+MgH_2$ mixture is very sensitive to the ball milling condition [33]. Ineffective ball milling suffers from severe caking problem, whereas effective ball milling eliminates caking. The ball milled powder with caking only releases less than 0.7 wt.% H_2 after holding at 265°C for 5 h. In contrast, the ball milled powder without caking can release as much as 4.0 wt.% H_2 under the same dehydriding condition, exhibiting a 5-fold increase in the amount of H_2 released [33]. This amount of H_2 released is the highest quantity released from the $2LiBH_4+MgH_2$ mixture in the solid state reported so far in the open literature [33]. The solid-state dehydrogenation of the $2LiBH_4+MgH_2$ mixture is found to be controlled by diffusion [34]. Thus, effective ball milling that can reduce particle sizes, introduce structural defects into crystalline MgH_2, and amorphize $LiBH_4$ can result in improvements in the solid-state dehydrogenation. Effective ball milling can be achieved via milling at liquid nitrogen temperature with the addition of 5 vol.% graphite into the $2LiBH_4+MgH_2$ mixture [33].

4.4 The reaction pathway of solid-state dehydrogenation of the $2LiBH_4 + MgH_2$ mixture: Reaction (13) has been proposed for the liquid state hydrogenation and dehydrogenation [26]. More detailed studies [35-38] reveal that the overall dehydrogenation reaction shown in Reaction (13) actually proceeds in two elementary steps as shown below.

$$MgH_2 \Rightarrow Mg + H_2 \qquad (16)$$

$$2LiBH_4 + Mg \Rightarrow 2LiH + MgB_2 + 3\,H_2 \qquad (17)$$

That is, MgH_2 decomposes first to generate atomic Mg which in turn reacts with $LiBH_4$ to form LiH and MgB_2 with release of H_2. However, our study [33] unveils that in the solid state the dehydrogenation of MgH_2 and $LiBH_4$ appears to proceed separately. Specifically, the hydrogen release of MgH_2 proceeds according to Reaction (16), whereas the hydrogen release of $LiBH_4$ may proceed according to Reaction (18). Although taking place separately, the two reactions or the reaction products from the two reactions appear to have a synergistic effect to enhance each other in releasing H_2 [33].

$$12\ LiBH_4\ (s) = Li_2B_{12}H_{12}\ (s) + 10\ LiH\ (s) + 13\ H_2\ (g) \qquad (18)$$

4.5 Enhancing hydriding and dehydriding reactions via transition metals: For micrometer-sized MgH_2 and $LiBH_4$ particles, the hydrogenation and dehydrogenation of their mixtures in the solid state are diffusion-controlled. Therefore, one of the methods to enhance H_2 uptake and release is to improve the diffusion coefficient. This can be done by doping the proper element to increase the lattice distortion and thus the diffusion coefficient. Thus, Mn and V dopants have been investigated. It is found that Mn addition to the $LiH + MgB_2$ mixture through high-energy ball milling enhances the hydriding reaction because of the formation of

the MgB_2 solid solution containing Mn element, which increases the diffusion rate of Mg ions in MgB_2 [34]. However, the dissolved Mn does not have effect on the dehydriding reaction rate. In contrast, V addition improves the dehydriding rate of the $LiBH_4$ + MgH_2 mixture because V forms $VH_{0.81}$ in the hydriding process [34]. $VH_{0.81}$ acts as a hydrogen pump to strip hydrogen from MgH_2, leading to the formation of Mg which subsequently reacts with $LiBH_4$. However, V does not enhance the hydriding reaction because it does not induce much lattice distortion in MgB_2 [39].

4.6 Enhancing hydriding and dehydriding reactions via graphite addition: Graphite addition offers the improvement in both hydriding and dehydriding rates of the $LiBH_4$ + MgH_2 system [40]. The improvement is achieved though several mechanisms (Fig. 11). First, graphite dissolves into MgB_2 to form a solid solution. This may increase the diffusion rate of Mg ions. Second, graphite is trapped at the interface of MgB_2 crystals and LiH crystals. The presence of graphite results in more open structures at the interface of MgB_2 crystals and thus increases the diffusion rate of Mg ions at the interface. This leads to higher hydriding kinetics as well as faster dehydriding rates. Finally, the dehydriding rate is also improved by the presence of graphite because C enhances the decomposition of MgH_2, thereby producing atomic Mg at a faster rate that subsequently reacts with $LiBH_4$.

4.7 The phenomenon of the storage capacity decrease in the graphite-containing LiH + MgB_2 system: In addition to enhancing hydriding and dehydriding kinetics, mechanically activated graphite also reacts with LiH during ball milling of the LiH + MgB_2 mixture [40]. This reaction degrades the storage capacity of the $LiBH_4$ + MgH_2 system because of the consumption of LiH. Thus, to fully utilize the beneficial effects of graphite and at the same time suppress the reaction between graphite and LiH, a two-stage ball milling procedure has been developed [40]. The $LiBH_4$ + MgH_2 system with graphite processed through the two-stage ball milling procedure exhibits the highest hydrogen uptake ever achieved with the $LiBH_4$ + MgH_2 system during continuous heating from ambient to 265^0C. The same system also displays the largest hydrogen release ever reported for the $LiBH_4$ + MgH_2 system with holding at 265^0C [40].

4.8 Enhancing hydriding and dehydriding reactions of the $LiBH_4$+MgH_2 system via nanoscale $LiBH_4$: Nanoscale $LiBH_4$ can start to release H_2 at ~35^oC as shown in Section III. Thus, to enhance the hydriding and dehydriding rates of the $LiBH_4$+MgH_2 mixture, we have infiltrated the submicrometer-sized MgH_2 powder using the $LiBH_4$/THF solution to form a thin coating of the nanoscale $LiBH_4$ on the surface of MgH_2 particles. Figure 12 shows the TGA data for the as-received MgH_2 powder, the ball milled MgH_2+10vol.%C mixture (i.e., the submicrometer-sized MgH_2), and the nanoscale $LiBH_4$ infiltrated MgH_2+10vol.%C mixture. The corresponding H_2 intensities from the effluent gases of all the samples as a function of temperature and time are also included in Fig. 12.

Several interesting phenomena are noted from Fig. 12. First, the behavior of the as-received MgH_2 is consistent with the expectation for 40μm particles and many other studies [41-48]; that is, appreciable H_2 release starts at ~250^oC and substantial H_2 release takes place near 400^oC. Second, the ball milled MgH_2 is very reactive. In fact, it is so reactive that it gets oxidized under a flowing argon atmosphere containing a small amount of residual oxygen

from air, leading to weight gain at the early stage of heating. However, near 300°C the hydrogen release from the ball milled MgH_2 becomes substantial and forms a H_2 gas blanket over the MgH_2 powder. As a result, oxidation stops because of the protection of the H_2 gas blanket, which leads to dramatic weight loss above 300°C. Third, all the samples exhibit weight gain after reaching or holding at 400°C for some times. This is ascribed to the oxidation of Mg (derived from the decomposition of MgH_2) by the residual oxygen in the flowing argon atmosphere. Note that all the weight gain events at 400°C are associated with a decrease in the hydrogen concentration in the effluent gas, supporting that the oxidation is related to the diminished capability of the Mg + MgH_2 mixture to release H_2 at 400°C. Fourth, the most exciting phenomenon from this set of experiments is the hydrogen release behavior of the nanoscale $LiBH_4$ infiltrated MgH_2+10%C powder (*c* curves in Fig. 12). This powder exhibits weight loss at ~35°C because of the H_2 release from the nanoscale $LiBH_4$ which forms a H_2 gas blanket to prevent oxidation of the MgH_2 powder. A close examination of the RGA data shown in Figs. 12 and 13 reveals that the gas evolved is indeed H_2 with no emission of THF and borane (B_2H_6). Although no THF and borane emissions are found, CH_4 formation at the high temperature range (> 325°C) has been identified. This is due to the reaction between the H_2 released and the carbon present in the starting powder. Fifth, the nanoscale $LiBH_4$ infiltrated MgH_2+10%C powder shows an accelerated weight loss at ~150°C. Based on the quantity of $LiBH_4$ present in the powder (6 vol.% only), we conclude that this weight loss is due to release of H_2 from MgH_2 because the total weight loss contributed by all the nanoscale $LiBH_4$ can only reach 0.43%.

The phenomena 4 and 5 mentioned above are technologically important because MgH_2 has never exhibited release of a large amount of H_2 at 150°C. All the reports in the open literature [41-48] show that 300°C is needed for substantial release of H_2 from MgH_2. Our own data shown in Fig. 12 also supports that 300°C is necessary for large quantity release of H_2 from pure MgH_2. The participation of MgH_2 in releasing H_2 at 150°C or lower is supported by XRD analysis of the products after dehydrogenation. As shown in Fig. 14, Mg is present in the products of the nanoscale $LiBH_4$ infiltrated MgH_2+10%C powder after dehydrogenation at either 150 or 265°C. Thus, our data unambiguously reveals that the presence of nanoscale $LiBH_4$ on the surface of MgH_2 can reduce the peak release temperature of MgH_2 from ~300°C to 150°C.

This discovery creates a new paradigm for the $LiBH_4$+MgH_2 system. Otherwise, this system does not have a chance to release a large quantity of H_2 at temperatures below 250°C because the reaction pathway of the micrometer-sized $LiBH_4$+MgH_2 mixture relies on the H_2 release from MgH_2 first, as shown in Reactions (16) and (17). The extensive studies over the last 40 years have shown that MgH_2 cannot release a large amount of H_2 at temperatures below 250°C [41-48]. As such, the micrometer-sized $LiBH_4$+MgH_2 mixture can only release a large amount of H_2 at temperatures above 250°C since it requires MgH_2 to release H_2 first. Our discovery with the nanoscale $LiBH_4$ infiltrated MgH_2 system has changed this grim situation completely. The nanoscale $LiBH_4$ can start to release H_2 at ~35°C. The product from the dehydrogenation of the nanoscale $LiBH_4$ can, in turn, catalyze the dehydrogenation of MgH_2, leading to a large amount of H_2 release from MgH_2 at 150°C.

Publications from This Project:

1) K. Crosby and L. Shaw, "Dehydriding and Rehydriding Properties of High-Energy Ball Milled $LiBH_4$ + MgH_2 Mixtures," *Int. J. Hydrogen Energy*, in press.
2) L. Shaw, X. Wan, J. Z. Hu, J. H. Kwak, and Z. Yang, "The Solid-State Hydriding Mechanism in the $LiBH_4$ + MgH_2 System," *J. Phys. Chem. C,* in press.
3) X. Wan, D. Goberman, L. Shaw, G. Yi, and G.-M. Chow, "Valence States of Nanocrystalline Ceria under Combined Effects of Hydrogen Reduction and Particle Size," *Appl. Phys. Lett.*, 96, 123108 (2010).
4) J.-Z. Hu*, J.-H. Kwak, Z. Yang, X. Wan, and L. Shaw, "Detailed Investigation of Ion Exchange in Ball Milled LiH+MgB_2 System using Ultra-High Field NMR Spectroscopy," *J. Power Sources*, 195, 3645–3648 (2010).
5) T. Markmaitree and L. Shaw, "Synthesis and Hydriding Properties of $Li_2Mg(NH)_2$," *J. Power Sources,* 195, 1984–1991 (2010).
6) W. Osborn, T. Markmaitree, L. Shaw, J. Z. Hu, J. H. Kwak, and Z. G. Yang, "Low Temperature Milling of the $LiNH_2$ + LiH Hydrogen Storage System," *Int. J. Hydrogen Energy*, 34, 4331-4339 (2009).
7) W. Osborn, T. Markmaitree, L. Shaw, R. Ren, J. Z. Hu, J. H. Kwak, and Z. G. Yang, "Solid-State Hydrogen Storage: Storage Capacity, Thermodynamics, and Kinetics," *JOM*, 61 [4] 45-51 (2009).
8) W. Osborn, T. Markmaitree, and L. Shaw, "Long-Term Hydriding and Dehydriding Stability of the Nanoscale $LiNH_2$ + LiH Hydrogen Storage System," *Nanotechnology*, 20, 204028 (2009).
9) J. Z. Hu, J. H. Kwak, Z. Yang, X. Wan, and L. Shaw, "Direct Observation of Ion Exchange in Mechanically Activated LiH+MgB_2 System Using Ultra-High Field Nuclear Magnetic Resonance Spectroscopy," *Appl. Phys. Lett.*, 94, 141905 (2009).
10) X. Wan, T. Markmaitree, W. Osborn, and L. Shaw, "Nanoengineering-Enabled Solid-State Hydrogen Uptake and Release in the $LiBH_4$ plus MgH_2 System," *J. Phys. Chem. C*, 112, 18232-18243 (2008).
11) J. Z. Hu, J. H. Kwak, Z. G. Yang, W. Osborn, T. Markmaitree, and L. Shaw, "Investigation of Mechanical Activation on Li-N-H Systems using ^{6}Li MAS NMR at Ultrahigh Field," *J. Power Sources*, 182, 278-283 (2008).
12) J. Z. Hu, J. H. Kwak, Z. G. Yang, W. Osborn, T. Markmaitree, and L. Shaw, "Probing the Reaction Pathway of Dehydrogenation of the $LiNH_2$ + LiH Mixture using In-Situ 1H NMR Spectroscopy," *J. Power Sources*, 181, 116-119 (2008).
13) T. Markmaitree, W. Osborn and L. Shaw, "Comparison between MgH_2- and LiH-Containing Systems for Hydrogen Storage Applications," *Int. J. Hydrogen Energy*, 33, 3915-3924 (2008)
14) T. Markmaitree, W. Osborn, and L. Shaw, "Comparative Studies of Reaction Rates of NH_3 with LiH and MgH_2," *J. Power Sources*, 180, 535-538 (2008).
15) A. Ortiz, W. Osborn, T. Markmaitree and L. Shaw, "Crystallite Sizes of LiH before and after Ball Milling and Thermal Exposure," *J. Alloys Compd.*, 454 [1-2] 297-305 (2008).
16) L. Shaw, W. Osborn, T. Markmaitree, and X. Wan, "The Reaction Pathway and Rate-Limiting Step of Dehydrogenation of $LiHN_2$ + LiH Mixture," *J. Power Sources*, 177, 500-505 (2008).

17) L. Shaw, R. Ren, T. Markmaitree, and W. Osborn, "Effects of Mechanical Activation on Dehydrogeneation of the Lithium Amide and Hydride System," *J. Alloys Compd.*, 448, 263-271 (2008).
18) C. Lu, J. Hu, J. H. Kwak, Z. G. Yang, R. Ren, T. Markmaitree, and L. Shaw, "Study the Effects of Mechanical Activation on Li-N-H Systems with ^{1}H and ^{6}Li Solid-State NMR," *J. Power Sources*, 170 [2] 419-424 (2007).
19) W. Osborn, T. Markmaitree and L. Shaw, "Evaluation of the Hydrogen Storage Behavior of a $LiNH_2$-MgH_2 System with a 1:1 Ratio," *J. Power Sources*, 172, 376-378 (2007).
20) T. Markmaitree, R. Ren, and L. Shaw, "Enhancement of Lithium Amide to Lithium Imide Transition via Mechanical Activation," *J. Phys. Chem. B.*, 110 [41] 20710-20718 (2006).
21) R. Ren, A. L. Ortiz, T. Markmaitree, W. Osborn, and L. Shaw, "Stability of Lithium Hydride in Argon and Air," *J. Phys. Chem. B.*, 110 [21] 10567-10575 (2006).

Presentations from This Project:

1) L. Shaw, "Enhancing Hydrogen Storage Properties through Nanoscale $LiBH_4$," **The John & Virginia Towers Distinguished Lecture**, Michigan Technological University, April 9, 2010.
2) L. Shaw, X. Wan, Y. Zhong, and K. Crosby, "Novel Hydrogen Storage Properties Derived from Nanoscale $LiBH_4$," **Invited Presentation** in the Conference of "Materials Challenges in Alternative & Renewable Energy 2010," Cocoa Beach, Florida, February 21-25, 2010.
3) L. Shaw, "The Pathways to On-Board Hydrogen Storage for Fuel Cell Vehicles," **Invited Presentation** at the Institute of Materials Science (IMS) Associates Program Annual Meeting, UConn, May 27, 2010.
4) R. Ren, T. Markmaitree, W. Osborn, L. Shaw, and Z. Yang, "Effects of Mechanical Activation on Dehydrogeneation of the Lithium Amide and Lithium Hydride System," **Invited Presentation** at the symposium on "Materials in Clean Powder System II: Fuel Cells, solar, and Hydrogen Based Technologies" in the TMS 2007 Annual Meeting, Orlando, FL, Feb 25 – March 1, 2007.
5) L. Shaw, "Nanostructured Lithium Amide and Lithium Hydride for Reversible Hydrogen Storage Applications," **Invited Presentation**, WPI, April 18, 2007.
6) L. Shaw, "Hydrogen Economy and Materials Issues," **Invited Presentation** at the ASM Hartford Chapter meeting, Hartford, CT, January 6, 2006.
7) X. Wan, K. Crosby, Y. Zhong, and L. Shaw, "Enhancing the Hydriding and Dehydriding Kinetics of $LiBH_4$+MgH_2 systems via the Addition of Transition Metals," presented in the Conference of "Materials Challenges in Alternative & Renewable Energy 2010," Cocoa Beach, Florida, February 21-25, 2010.
8) L. Shaw, M. Utz, Z. G. Yang, R. Ren, T. Markmaitree and H. Luo, "Lithium Nitride-Based Materials for Hydrogen Storage," in CD-ROM of the 2005 Annual DOE Hydrogen Program Review Meeting, Washington D.C., May 23 – 26, 2005.

9) R. Ren, T. Markmaitree, L. Shaw, and Z. Gary Yang, "Effects of Mechanical Activation on Lithium Amide/Imide Transition and Hydrogen Sorption/Desorption," presented at the Symposium on Materials for the Hydrogen Economy held in MS&T '05, Pittsburgh, PA, September 25 - 28, 2005.
10) L. Shaw, Z. G. Yang, R. Ren, T. Markmaitree and W. Osborn, "Effect and Mechanisms of Mechanical Activation on Hydrogen Sorption/Desorption of Nanoscale Lithium Nitrides," in CD-ROM of the 2006 Annual DOE Hydrogen Program Review Meeting, Washington D.C., May 16 – 19, 2006.
11) C. Lu, J. Y. Kim, Z. Yang and L. Shaw, "Hydrogen Storage Characteristics of Lithium Nitride Based Materials," presented at the symposium on "Materials and Devices for Energy Harvesting, Generation and Storage Systems" in MS&T '06, Cincinnati, Ohio, October 15-18, 2006.
12) C. Lu, J. Hu, Z. Yang, and L. Shaw, "NMR Study of Mechanically Activated Li-N-H System," presented at the symposium on "Materials in Clean Powder System II: Fuel Cells, solar, and Hydrogen Based Technologies" in the TMS 2007 Annual Meeting, Orlando, FL, Feb 25 – March 1, 2007.
13) C. Lu, J. Kim, Z. Yang, and L. Shaw, "Modification of Light Metal Complex Hydrides for Improved Storage Properties," presented at the symposium on "Materials in Clean Powder System II: Fuel Cells, solar, and Hydrogen Based Technologies" in the TMS 2007 Annual Meeting, Orlando, FL, Feb 25 – March 1, 2007.
14) L. Shaw, T. Markmaitree, W. Osborn, X. Wan, Z. G. Yang, J. Hu, C. Lu, and J. Liu, "Effect and Mechanisms of Mechanical Activation on Hydrogen Sorption/Desorption of Nanoscale Lithium Nitrides," in CD-ROM of the 2007 Annual DOE Hydrogen Program Review Meeting, Washington D.C., May 15 – 18, 2007.
15) T. Markmaitree, W. Osborn, and L. Shaw, "Comparisons between MgH_2– and LiH-Containing Systems for Hydrogen Storage Applications," presented in the Symposium on "Materials and Technology for Hydrogen Storage" at MRS 2007 Fall Meeting, Boston, MA, November 26 - 30, 2007.
16) W. Osborn, T. Markmaitree, L. Shaw, J. Hu, Z. Gary Yang, "Low Temperature Milling of the Lithium Hydride and Amide Hydrogen Storage System," presented in the Symposium on "Materials and Technology for Hydrogen Storage" at MRS 2007 Fall Meeting, Boston, MA, November 26 - 30, 2007.
17) L. Shaw, W. Osborn, T. Markmaitree, and X. Wan, "The Reaction Pathway and Rate-Limiting Step of Dehydrogenation of the $LiHN_2$ + LiH Mixture," presented in the Symposium on "Materials and Technology for Hydrogen Storage" at MRS 2007 Fall Meeting, Boston, MA, November 26 - 30, 2007.
18) W. Osborn, T. Markmaitree, L. Shaw, and Z. Gary Yang, "Long-Term Cyclic Stability of Lithium Amide and Hydride Systems for Hydrogen Storage Applications," presented in the Symposium on "Fuel Cells: Materials, Processing, Manufacturing and Power Management Technologies" at the MS&T 2007 Conference in Detroit, Michigan, September 16 – 20, 2007.
19) W. Osborn, T. Markmaitree, X. Wan, L. Shaw, and Z. Gary Yang, "Hydrogen Uptake and Release Behavior of Lithium Amide and Hydride Systems for Hydrogen Storage Applications," presented in the Symposium on "Materials in Clean Power Systems III: Fuel Cells, Hydrogen-, and Clean Coal-Based Technologies" at the TMS 2008 Annual Meeting, New Orleans, Louisiana, March 9 – 13, 2008.

20) L. Shaw, T. Markmaitree, W. Osborn, X. Wan, K. Crosby, Z. G. Yang, J. Z. Hu, and J. H. Kwak, "Effects and Mechanisms of Mechanical Activation on Hydrogen Sorption/Desorption of Nanoscale Lithium Nitrides," presented at the FreedomCAR and Fuel Hydrogen Storage Technical Team Meeting, Detroit, MI, May 14, 2008.
21) X. Wan, T. Markmaitree, W. Osborn, K. Crosby, L. Shaw, "Nanoengineering-Enabled Solid-State Hydrogen Uptake and Release in the $LiBH_4$ plus MgH_2 System," presented in the symposium of "Energy Materials" at the MS&T 2009 Meeting, Pittsburgh, Pennsylvania, October 25 – 29, 2009.

References Cited:

1) P. Chen, Z. Xiong, J. Z. Luo, J. Y. Lin, K. L. Tan, Interaction of hydrogen with metal nitrides and imides, *Nature*, 420, 302-304 (2002).
2) L. Shaw, W. Osborn, T. Markmaitree, and X. Wan, "The Reaction Pathway and Rate-Limiting Step of Dehydrogenation of $LiHN_2$ + LiH Mixture," *J. Power Sources*, 177, 500-505 (2008).
3) L. Shaw, R. Ren, T. Markmaitree, and W. Osborn, "Effects of Mechanical Activation on Dehydrogeneation of the Lithium Amide and Hydride System," *J. Alloys Compd.*, 448, 263-271 (2008).
4) J. Z. Hu, J. H. Kwak, Z. G. Yang, W. Osborn, T. Markmaitree, and L. Shaw, "Probing the Reaction Pathway of Dehydrogenation of the $LiNH_2$ + LiH Mixture using In-Situ 1H NMR Spectroscopy," *J. Power Sources*, 181, 116-119 (2008).
5) Ichikawa T, Hanada N, Isobe S, Leng H, Fujii H. Mechanism of novel reaction from $LiNH_2$ and LiH to Li_2NH and H_2 as a promising hydrogen storage system, J. Phys. Chem. B, 2004, 108, 7887-7892.
6) Yao JH, Shang C, Aguey-Zinsou KF, Guo ZX. Desorption characteristics of mechanically and chemically modified $LiNH_2$ and ($LiNH_2$ + LiH), J. Alloys Comp., 2007, 432, 277-282.
7) T. Markmaitree, R. Ren, and L. Shaw, "Enhancement of Lithium Amide to Lithium Imide Transition via Mechanical Activation," *J. Phys. Chem. B.*, 110 [41] 20710-20718 (2006).
8) L. Shaw, T. Markmaitree, W. Osborn, X. Wan, Z. G. Yang, J. Hu, and J.H. Kwak, "Effect and mechanisms of mechanical activation on hydrogen sorption/desorption of nanoscale lithium nitrides," DOE quarterly report, December 2007.
9) C. Lu, J. Hu, J. H. Kwak, Z. G. Yang, R. Ren, T. Markmaitree, and L. Shaw, "Study the Effects of Mechanical Activation on Li-N-H Systems with ^{1}H and ^{6}Li Solid-State NMR," *J. Power Sources*, 170 [2] 419-424 (2007).
10) J. Z. Hu, J. H. Kwak, Z. G. Yang, W. Osborn, T. Markmaitree, and L. Shaw, "Investigation of Mechanical Activation on Li-N-H Systems using ^{6}Li MAS NMR at Ultrahigh Field," *J. Power Sources*, 182, 278-283 (2008).
11) A. Ortiz, W. Osborn, T. Markmaitree and L. Shaw, "Crystallite Sizes of LiH before and after Ball Milling and Thermal Exposure," *J. Alloys Compd.*, 454 [1-2] 297-305 (2008).
12) W. Osborn, T. Markmaitree, L. Shaw, J. Z. Hu, J. H. Kwak, and Z. G. Yang, "Low Temperature Milling of the $LiNH_2$ + LiH Hydrogen Storage System," *Int. J. Hydrogen Energy*, 34, 4331-4339 (2009).

13) W. Osborn, T. Markmaitree, and L. Shaw, "Long-Term Hydriding and Dehydriding Stability of the Nanoscale $LiNH_2$ + LiH Hydrogen Storage System," *Nanotechnology*, 20, 204028 (2009).
14) T. Markmaitree, W. Osborn and L. Shaw, "Comparison between MgH_2- and LiH-Containing Systems for Hydrogen Storage Applications," *Int. J. Hydrogen Energy,* 33, 3915-3924 (2008)
15) T. Markmaitree, W. Osborn, and L. Shaw, "Comparative Studies of Reaction Rates of NH_3 with LiH and MgH_2," *J. Power Sources,* 180, 535-538 (2008).
16) T. Markmaitree and L. Shaw, "Synthesis and Hydriding Properties of $Li_2Mg(NH)_2$," *J. Power Sources*, 195, 1984–1991 (2010).
17) X. Wan and L. Shaw, "Novel dehydrogenation properties derived from nanoscale $LiBH_4$," *Adv. Funct. Mater*., submitted April 2010.
18) E. M. Fedneva, V. L. Alpatova, and V. I. Mikheeva, "$LiBH_4$ complex hydride materials," *Russ. J. Inorg. Chem*., 9, 826-827 (1964).
19) A. Zuttel, S. Rentsch, P. Fischer, P. Wenger, P. Sudan, Ph. Mauron, and Ch. Emmenegger, "Hydrogen storage properties of $LiBH_4$," *J. Alloys Compd*., 356-357, 515-520 (2003).
20) A. Zuttel, P. Wenger, S. Rentsch, P. Sudan, Ph. Mauron, and Ch. Emmenegger, "$LiBH_4$ a new hydrogen storage material," *J. Power Sources*. 118, 1-7 (2003).
21) P. Mauron, F. Buchter, O. Friedrichs, A. Remhof, M. Bielmann, C. N. Zwicky, and A. Zuttel, "Stability and reversibility of $LiBH_4$," *J. Phys. Chem. B*, 112, 906-910 (2008).
22) J. Kostka, W. Lohstroh, M. Fichtner, and H. Hahn, "Diborane release from $LiBH_4$/silica-gel mixtures and the effect of additives," *J. Phys. Chem. C*, 111, 14026-14029 (2007).
23) Z. Z. Fang, P. Wang, T. E. Rufford, X. D. Kang, G. Q. Lu, and H. M. Cheng, "Kinetic- and thermodynamic-based improvements of lithium borohydride incorporated into activated carbon," *Acta Mater*., 56, 6257-6263 (2008).
24) Y. Zhang, W.-S. Zhang, A.-Q. Wang, L.-X. Sun, M.-Q. Fan, H.-L. Chu, J.-C. Sun, and T. Zhang, "$LiBH_4$ nanoparticles supported by disordered mesoporous carbon: hydrogen storage performances and destabilization mechanisms," *Int. J. Hydrogen Energy*, 32, 3976-3980 (2007).
25) A. Zuttel, A. Borgschulte, and S.-I. Orimo, "Tetrahydroborates as new hydrogen storage materials," *Scripta Mater*., 56, 823-828 (2007).
26) J. J. Vajo, S. L. Skeith, and F. Mertens, "Reversible storage of hydrogen in destabilized $LiBH_4$," *J. Phys. Chem. B*, 109, 3719-3722 (2005).
27) X, Wan, T. Markmaitree, W. Osborn, and L. Shaw, "Nanoengineering-enabled solid-state hydrogen uptake and release in the $LiBH_4$ plus MgH_2 system," *J. Phys. Chem. C*, 112, 18232-18243 (2008).
28) Z. Huang, J. Gallucci, X. Chen, T. Yisgedu, H. K. Lingam, S. Shore, and J.-C. Zhao, "$Li_2B_{12}H_{12}{\cdot}7NH_3$: a new ammine complex for ammonia storage or indirect hydrogen storage," *J. Mater. Chem*., in press.
29) S.-I. Orimo, Y. Nakamori, N. Ohba, K. Miwa, M. Aoki, S.-i. Towata, and A. Zuttel, "Experimental studies on intermediate compounds of $LiBH_4$," *Appl. Phys. Lett.*, 89, 021920 (2006).
30) J. Z. Hu, J. H. Kwak, Z. Yang, X. Wan, and L. Shaw, "Direct Observation of Ion Exchange in Mechanically Activated LiH+MgB_2 System Using Ultra-High Field Nuclear Magnetic Resonance Spectroscopy," *Appl. Phys. Lett.*, 94, 141905 (2009).

31) J.-Z. Hu, J.-H. Kwak, Z. Yang, X. Wan, and L. Shaw, "Detailed Investigation of Ion Exchange in Ball Milled LiH+MgB_2 System using Ultra-High Field NMR Spectroscopy," *J. Power Sources*, 195, 3645–3648 (2010).
32) L. Shaw, X. Wan, J. Z. Hu, J. H. Kwak, and Z. Yang, "The Solid-State Hydriding Mechanism in the $LiBH_4$ + MgH_2 System," *J. Phys. Chem. C,* in press.
33) K. Crosby and L. Shaw, "Dehydriding and Rehydriding Properties of High-energy Ball Milled $LiBH_4$ + MgH_2 Mixtures," *Int. J. Hydrogen Energy*, in press.
34) K. Crosby, "Studies of Lithium Borohydride-Based Solid State Hydrogen Storage Materials," MS Thesis, the University of Connecticut, 2009.
35) X. B. Yu, D. M. Grant, G. S. Walker, "A new dehydrogenation mechanism for reversible multicomponent borohydride systems – the role of Li-Mg alloys," Chem. Commun., (2006) 3906-3908.
36) F. E. Pinkerton, M. S. Meyer, G. P. Meisner, M. P. Balogh, J. J. Vajo, "Phase boundaries and reversibility of $LiBH_4$/MgH_2 hydrogen storage material," J. Phys. Chem. C 111, (2007) 12881-12885.
37) T. Nakagawa, T. Ichikawa, N. Hanada, Y. Kojima, H. Fujii, "Thermal analysis on the Li-Mg-B-H systems," J. Alloys Comp. 446-447, (2007) 306-309.
38) G. S. Walker, D. M. Grant, T. C. Price, X. B. Yu, V. Legrand, "High capacity multicomponent hydrogen storage materials: investigation of the effect of stoichiometry and decomposition conditions on the cycling behavior of $LiBH_4$-MgH_2," J. Power Sources 194, (2009) 1128-1134.
39) Y. Zhong, H. Zhu, L. Shaw and R. Ramprasad, "Ab-initio Computational Studies of Mg Vacancy Diffusion in Doped MgB_2 Aimed at Hydrogen Storage Applications," Chem. Commun., submitted April 2010.
40) L. Shaw, T. Markmaitree, W. Osborn, X. Wan, K. Crosby, Z. G. Yang, J. Z. Hu, and J. H. Kwak, "Effects and Mechanisms of Mechanical Activation on Hydrogen Sorption/Desorption of Nanoscale Lithium Nitrides," DOE Quarterly Report, December 2008.
41) Huang, Z. G.; Guo, Z. P.; Calka, A.; Wexler, D.; Wu, J.; Notten, P. H. L.; Liu, H. K. "Noticeable improvement in the desorption temperature from graphite in rehydrogenated MgH_2/graphite composite," *Mater. Sci. Eng. A* **2007**, 447, 180-185.
42) Bouaricha, S.; Dodelet, J. P.; Guay, D.; Huot, J.; Schulz, R. "Activation characteristics of graphite modified hydrogen absorbing materials," *J. Alloys Compd*. **2001**, 325, 245-251.
43) Guvendiren, M.; Bayboru, E.; Ozturk, T. "Effects of additives on mechanical milling and hydrogenatioin of magnesium powders," *Int. J. Hydrogen Energy* **2004**, 29, 491-496.
44) Wu, C. Z.; Wang, P.; Yao, X.; Liu, C.; Chen, D. M.; Lu, G. Q.; Cheng, H. M. "Hydrogen storage properties of MgH_2/SWNT composite prepared by ball milling," *J. Alloys Compd*. **2006**, 420, 278-282.
45) Zaluska, A.; Zaluski, L.; Strom-Olsen, J. O. "Structure, catalysis and atomic reactions on the nano-scale: a systematic approach to metal hydrides for hydrogen storage," *Appl. Phys. A* **2001,** 72, 157-165.
46) Huot, J.; Liang, G.; Schulz, R. "Mechanically alloyed metal hydride systems," *Appl. Phys. A* **2001**, 72, 187-195.

47) Tien, H.-Y.; Tanniru, M.; Wu, C.-Y.; Ebrahimi, F. “Effect of hydride nucleation rate on the hydrogen capacity of Mg,” *Int. J. Hydrogen Energy* **2009**, 34, 6343-6349.
48) Tanniru, M.; Ebrahimi, F. “Effect of Al on the hydrogenation characteristics of nanocrystalline Mg powder,” *Int. J. Hydrogen Energy* **2009**, 34, 7714-7723.

Final Report

(December 9, 2004 – December 31, 2009)

Project Title: Effects and Mechanisms of Mechanical Activation on Hydrogen Sorption/ Desorption of Nanoscale Lithium Nitrides

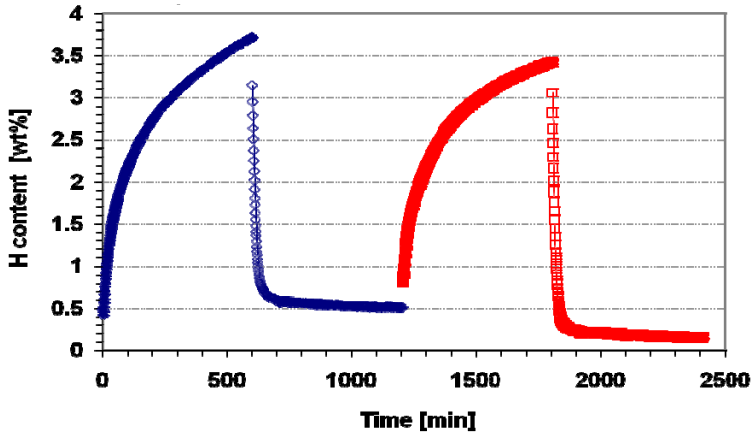

Figure 1: Isothermal hydrogen uptake/release cycles of the $Mg(NH_2)_2$ + 2LiH system at 200°C with a hydrogen pressure of 68 bars for hydriding and 0.03 bars for dehydriding. Note the dehydrogenation is very fast, whereas the hydrogenation is very sluggish.

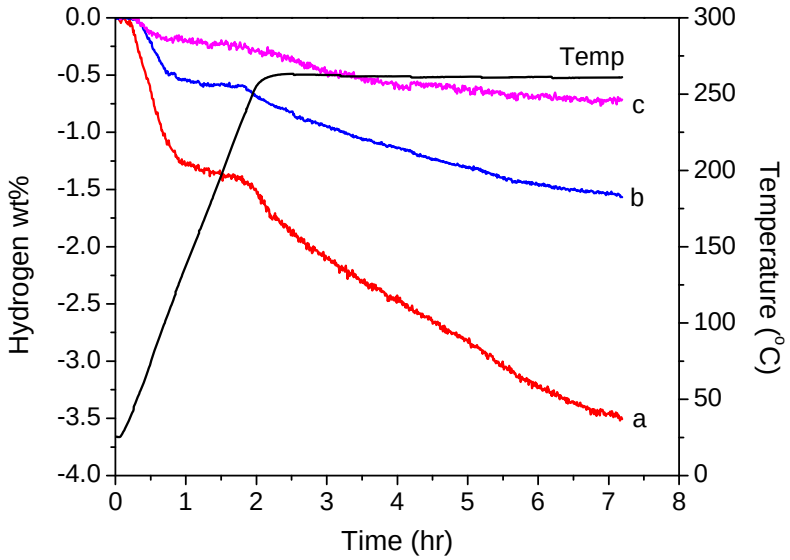

Figure 2. A comparison of the dehydrogenation curves of two nanoscale $LiBH_4$ powders derived from the $LiBH_4$/THF solution with the as-purchased bulk $LiBH_4$ powder. (a) Nanoscale $LiBH_4$ powder without oxidation, (b) nanoscale $LiBH_4$ powder with partial oxidation, and (c) the bulk $LiBH_4$ powder. Dehydrogenation was conducted in the PCT device under a vacuum of ~0.01 bar with a heating rate of 2°C/min from the ambient to 265°C and then holding at that temperature for 5 h.

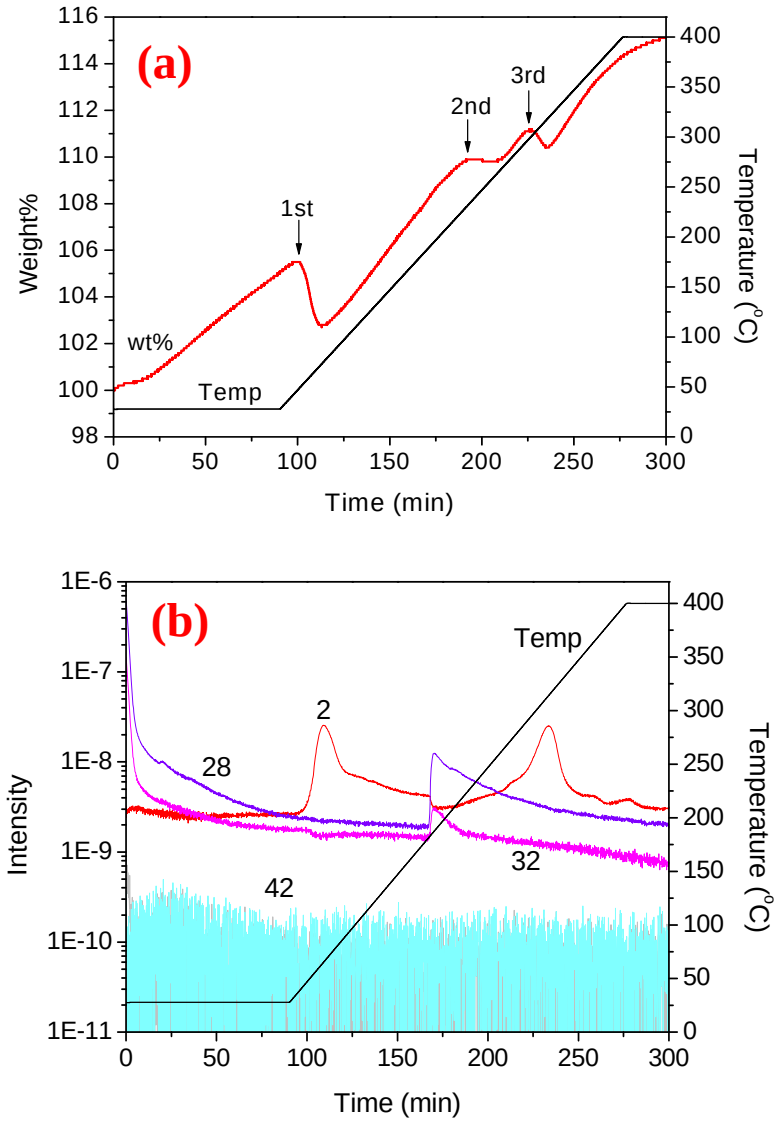

Figure 3. (a) The thermogravimetric analysis of the nanoscale $LiBH_4$ powder, and (b) the corresponding composition profile of the effluent gas. The signal with the mass-to-charge ratio of 2 is from H_2, 28 from both N_2 and CO, 32 from O_2 and 42 from THF. The signal from borane (27) is buried inside the signal of 42 and no change is found in the entire heating process. The sudden change for all signals at 170 min is due to the purging of argon into the glovebox that holds the TGA instrument. The holding and heating conditions are (i) holding at room temperature for 90 min, (ii) heating from ambient to 400°C with a rate of 2°C/min, and (iii) holding at 400°C for 25 min. A flowing argon atmosphere in the sample cell is maintained in the entire holding and heating process.

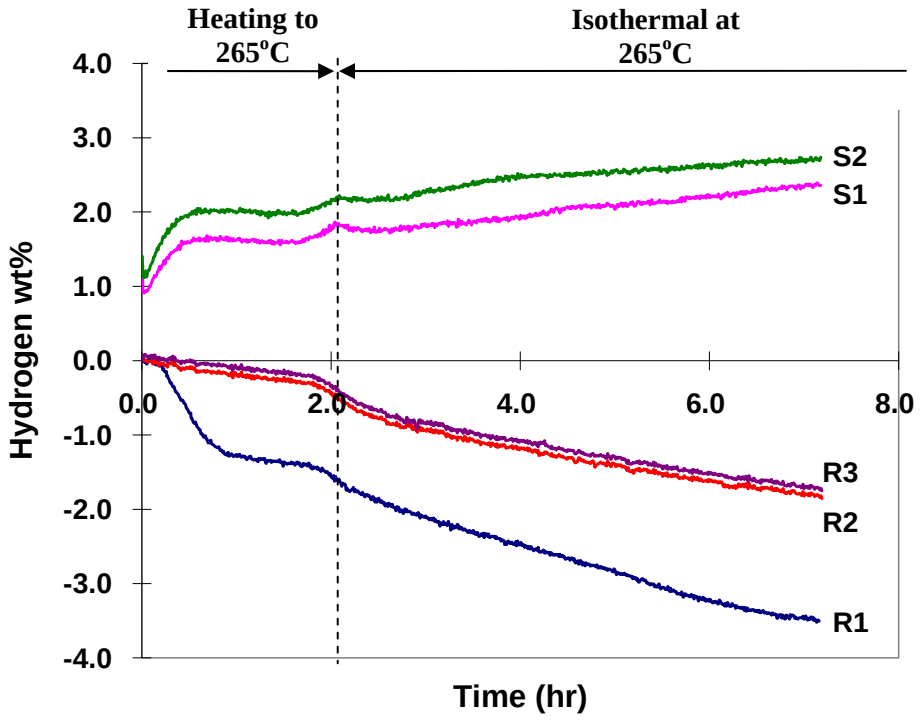

Figure 4. Dehydriding and re-hydriding curves of the nano-$LiBH_4$ powder. R1, R2 and R3 stand for the first, second and third hydrogen release in the PCT device (under a vacuum of ~0.001 MPa), whereas S1 and S2 represent the first and second re-hydrogenation (i.e., soak under a hydrogen pressure of 9 MPa). The heating rate and temperature profile (not shown here) are identical to those shown in Fig. 1.

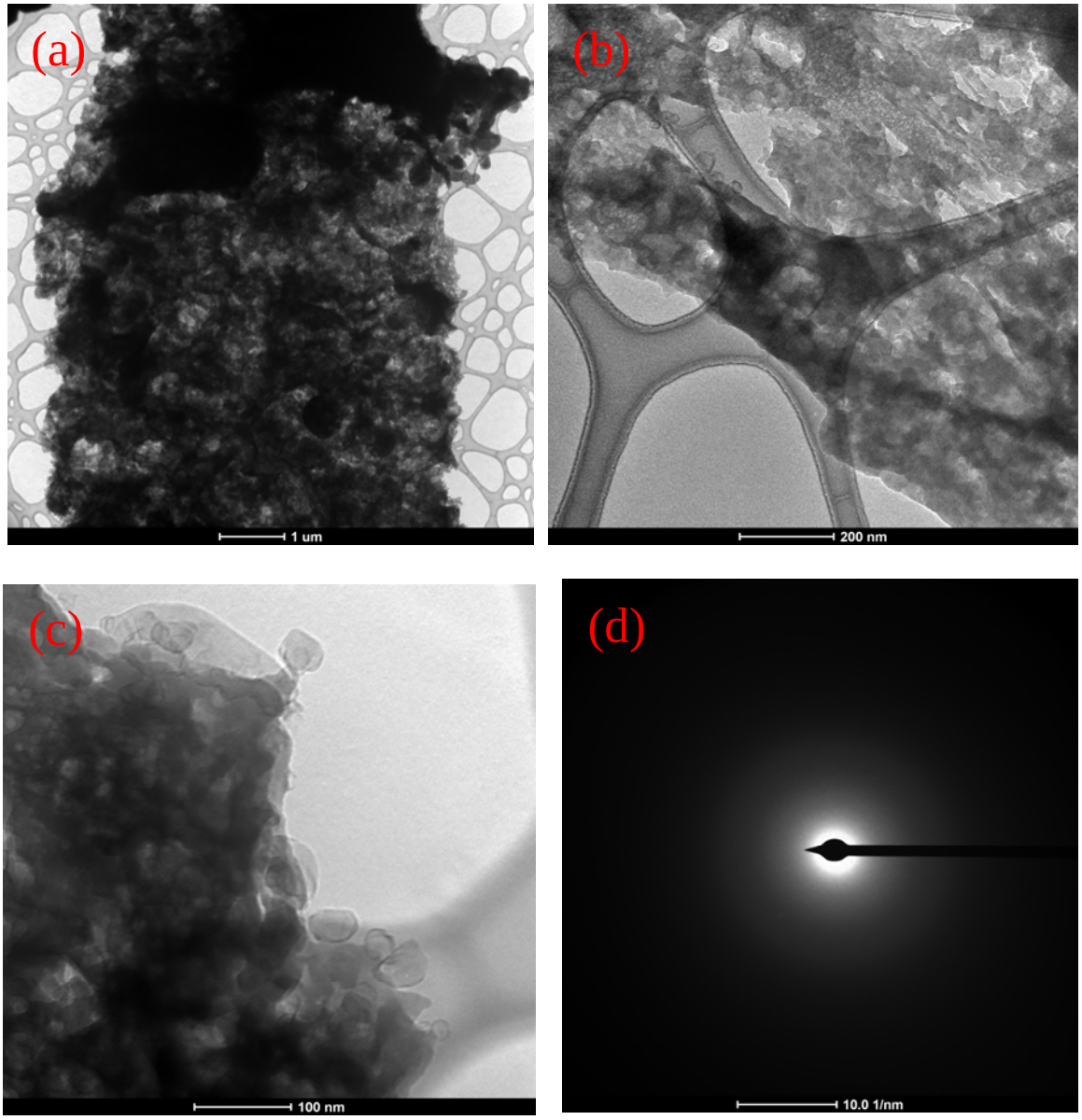

Figure 5. TEM images of the pure $LiBH_4$ powder derived from the $LiBH_4$/THF solution and its associated selected area diffraction (SAD) pattern. The pure $LiBH_4$ powder takes on several morphologies: (a) chucks, (b) thin films, and (c) particles. However, all of them contain extensive pores and are actually aggregates composed of ultrafine particles or basic units of irregular shapes of about 20 to 50 nm. The SAD pattern at (d) indicates the amorphous nature of the pure $LiBH_4$ powder.

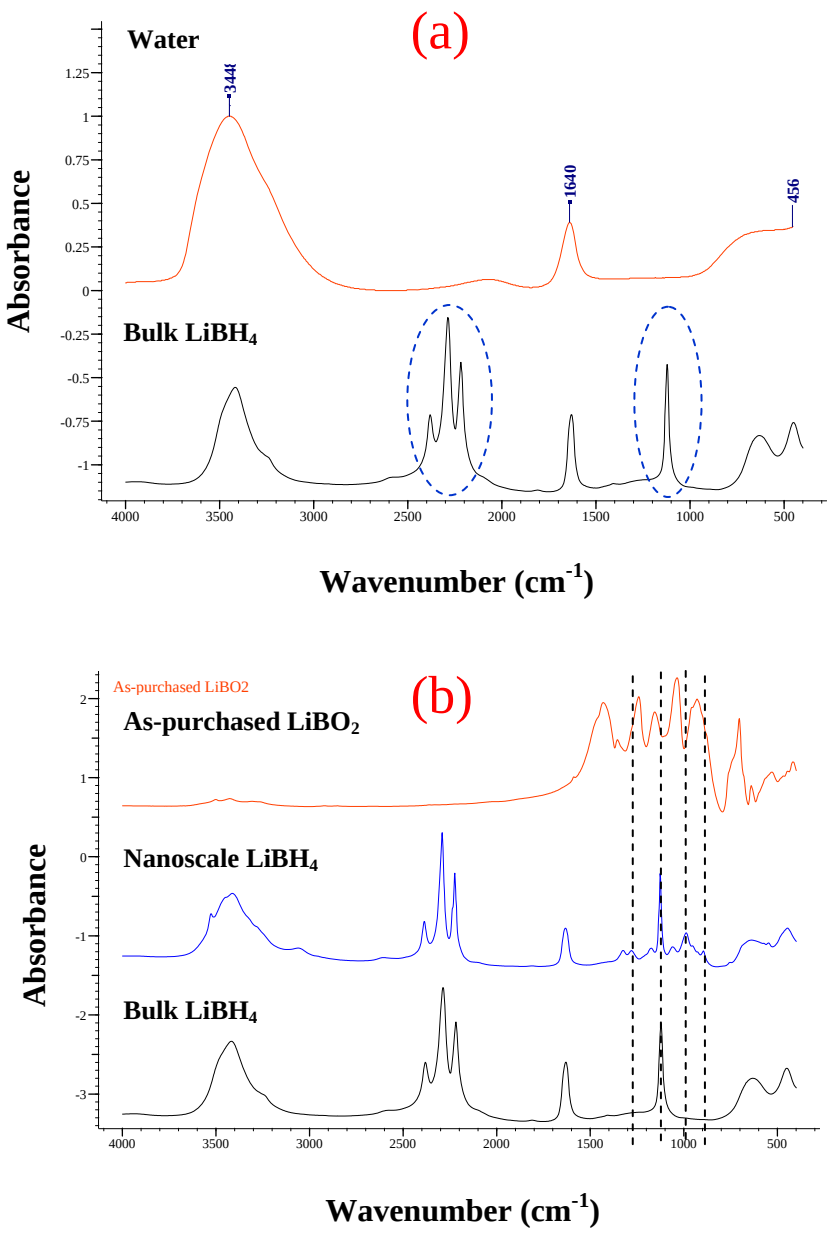

Figure 6. FTIR spectra of (a) the as-purchased bulk $LiBH_4$ powder and water, and (b) the nanoscale $LiBH_4$ derived from the $LiBH_4$/THF solution in comparison with the as-purchased bulk $LiBH_4$ and the as-purchased $LiBO_2$. The absorption peaks circled in (a) are the characteristic peaks of the $[BH_4]^-$ complex.

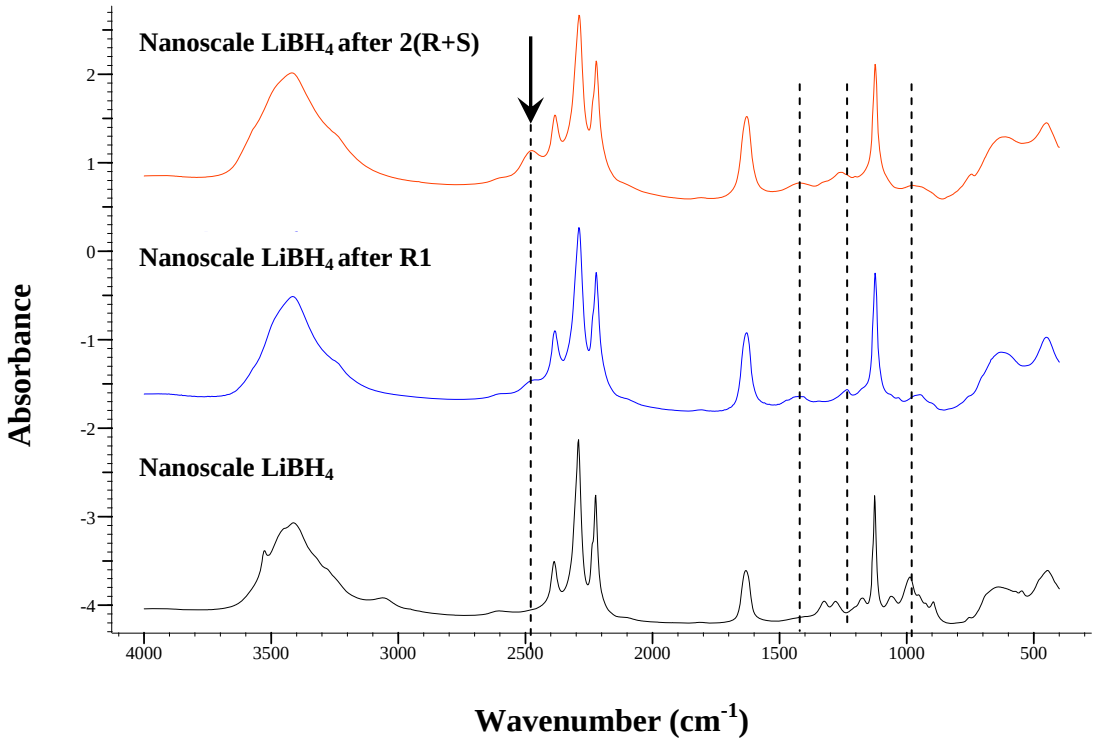

Figure 7. FTIR spectra of the nanoscale $LiBH_4$ derived from the $LiBH_4$/THF solution before and after the dehydrogenation and re-hydrogenation treatment at 265°C. R1 stands for one hydrogen release treatment, whereas 2(R+S) represents two hydrogen release/soak treatment. The temperature and pressure conditions for dehydrogenation and re-hydrogenation cycles are the same as those shown in Fig. 4. The arrow indicates the position of the frequency of the B-H stretching vibration from $Li_2B_{12}H_{12}$ identified previously in Ref. 28.

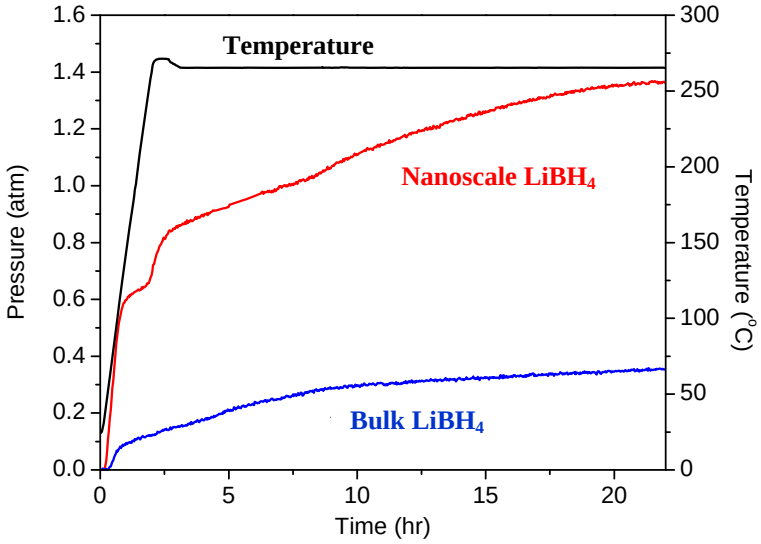

Figure 8. The dissociation pressure for the nanoscale $LiBH_4$ at 265°C in comparison with the dissociation pressure of the bulk $LiBH_4$. The leveling off in the pressure for both $LiBH_4$, when the holding time is larger than 20 h, suggests that the gas pressure is approaching the dissociation pressure for both samples.

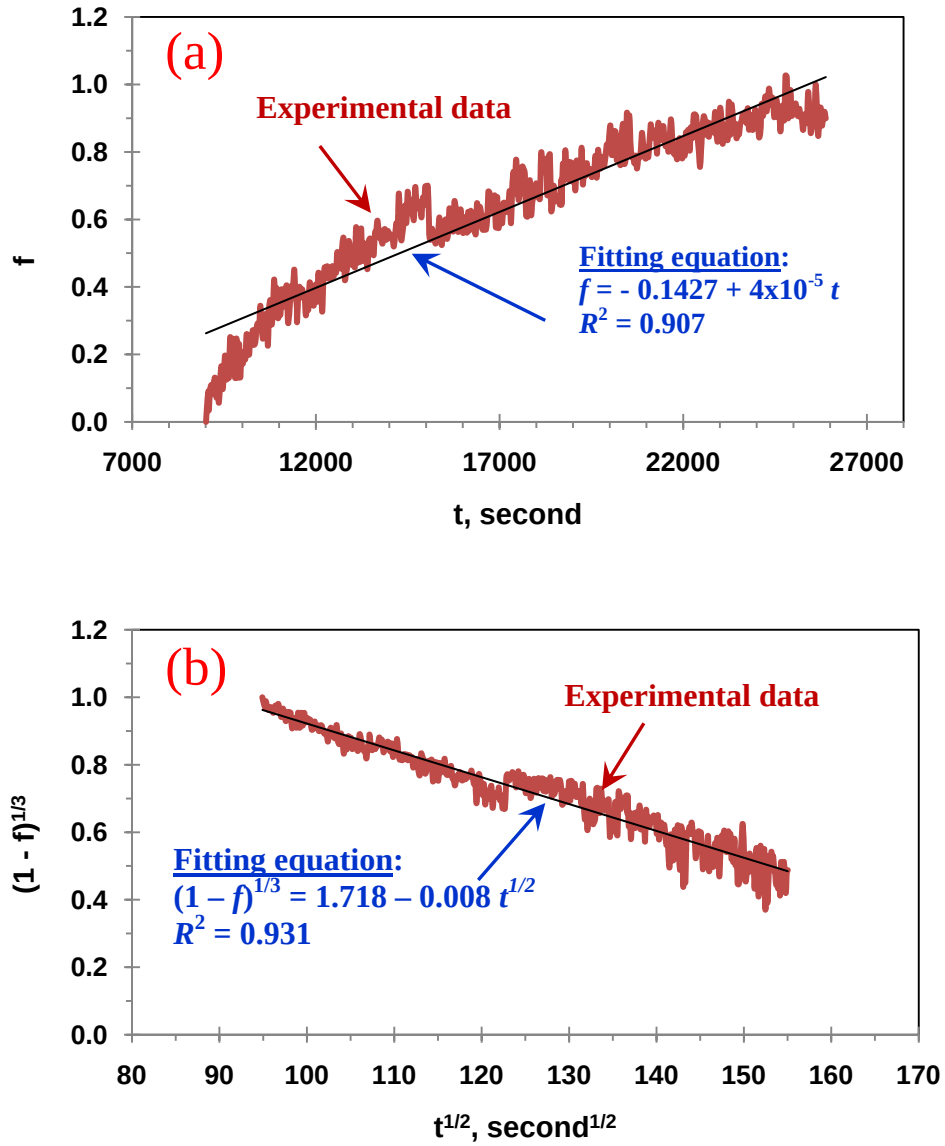

Figure 9. Analysis of the dehydrogenation curve of the bulk $LiBH_4$ at 265°C (i.e., curve *c* in Fig. 2): (a) curve fitting with dehydrogenation controlled by gas desorption at the surface of the $LiBH_4$ particle, and (b) curve fitting with dehydrogenation controlled by diffusion through a product shell formed on the surface of the $LiBH_4$ particle core. A good fit for the diffusion-controlled reaction is present, whereas the fit to the gas desorption-controlled reaction is very poor.

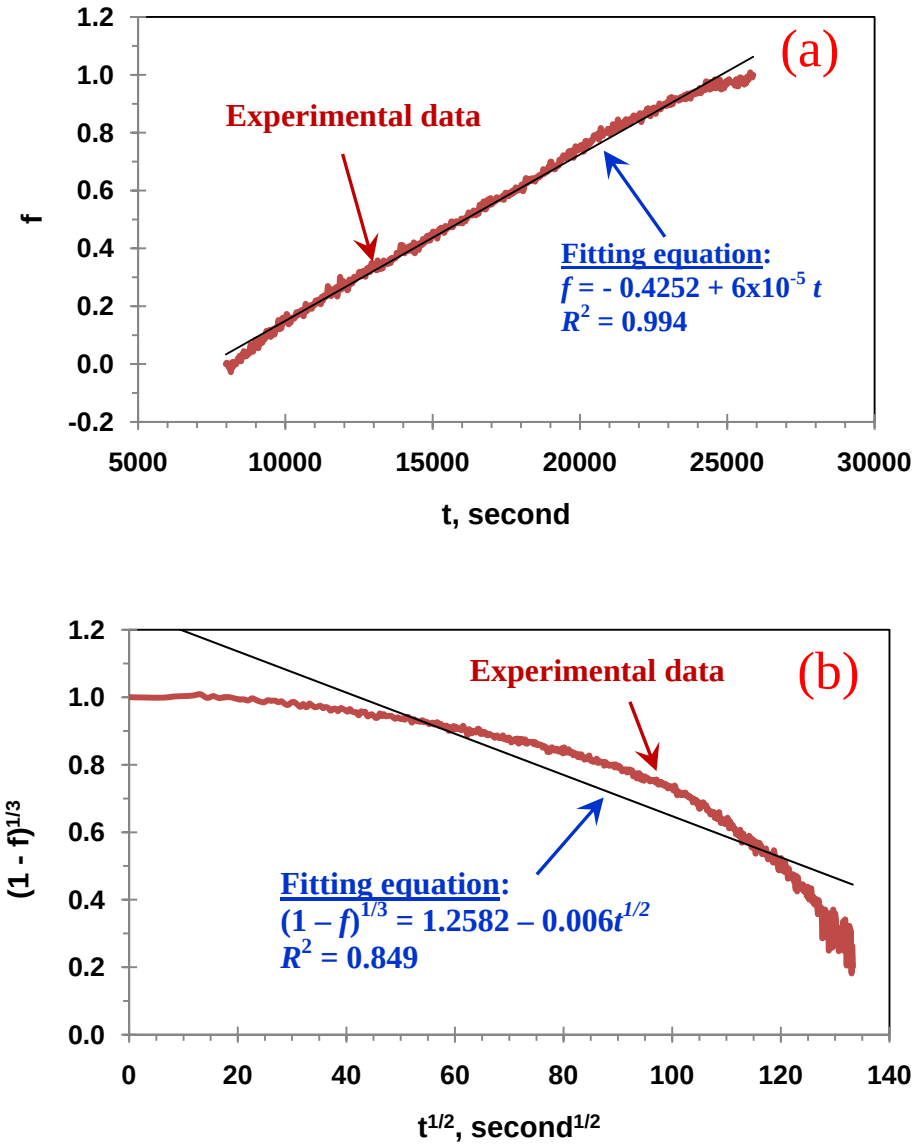

Figure 10. Analysis of the dehydrogenation curve of the nanoscale $LiBH_4$ at 265°C (i.e., curve *b* in Fig. 2): (a) curve fitting with dehydrogenation controlled by gas desorption at the surface of the $LiBH_4$ particle, and (b) curve fitting with dehydrogenation controlled by diffusion through a product shell formed on the surface of the $LiBH_4$ particle core. A good fit for the gas desorption-controlled reaction is present, whereas the fit to the diffusion-controlled reaction is very poor.

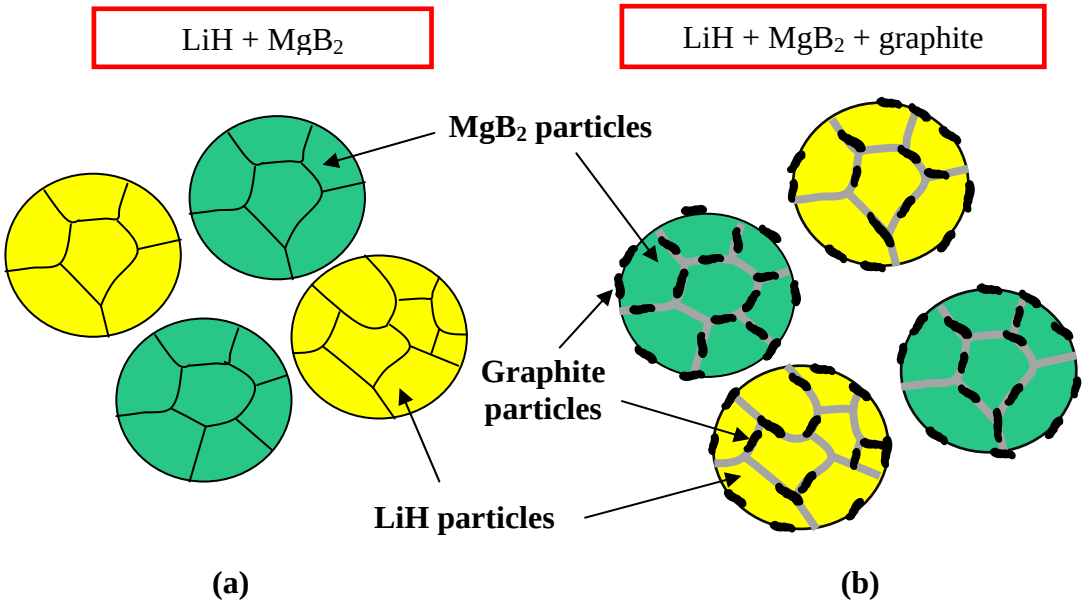

Figure 11. Schematic of ball milled LiH and MgB_2 mixtures: (a) without graphite and (b) with graphite. Note that graphite is present on the surface of nanostructured LiH and MgB_2 aggregates as well as at the interfaces within the aggregates. The presence of graphite at the interfaces within the aggregates is supported by NMR analysis and the specific surface area measurement.

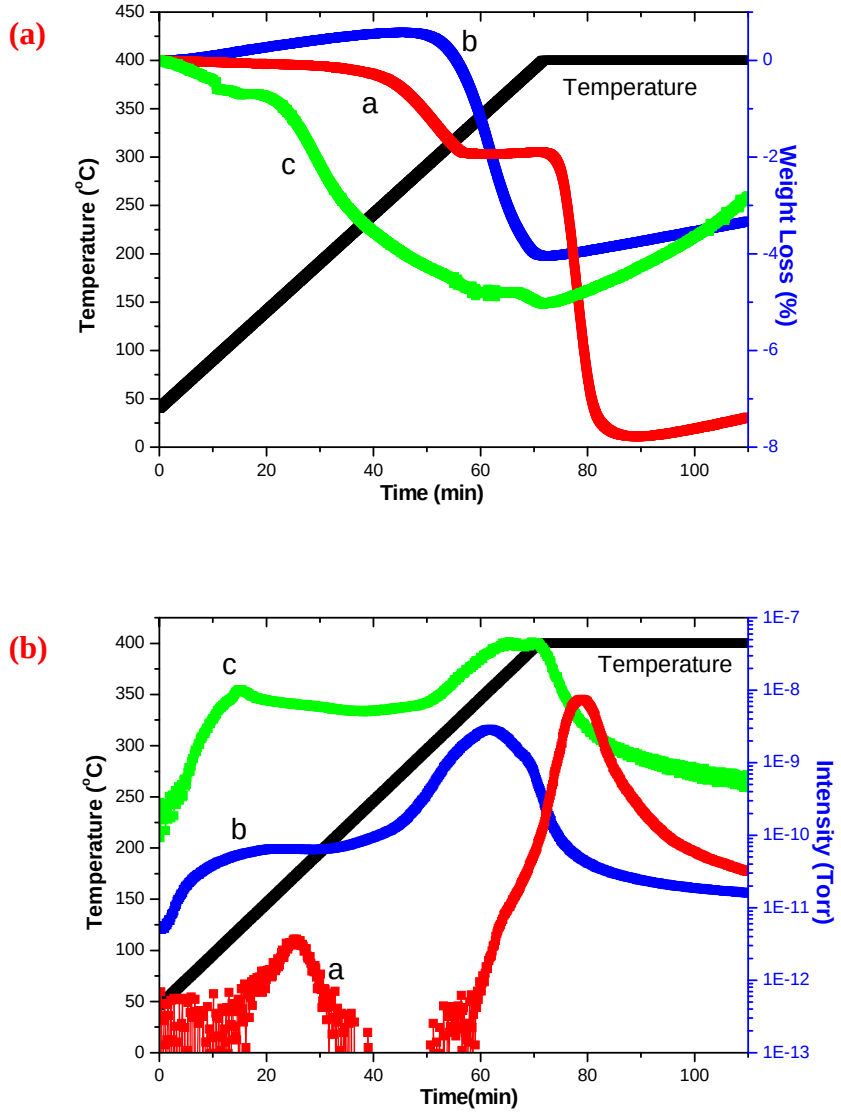

Figure 12. (i) The TGA curves and (ii) the corresponding effluent hydrogen prolifes along with the temperature curves for (a) the as-received commercial MgH_2 powder, (b) the ball milled MgH_2 + 10 vol.% C mixture, and (c) the nanoscale $LiBH_4$ infiltratated MgH_2 + 10 vol.% C mixture.

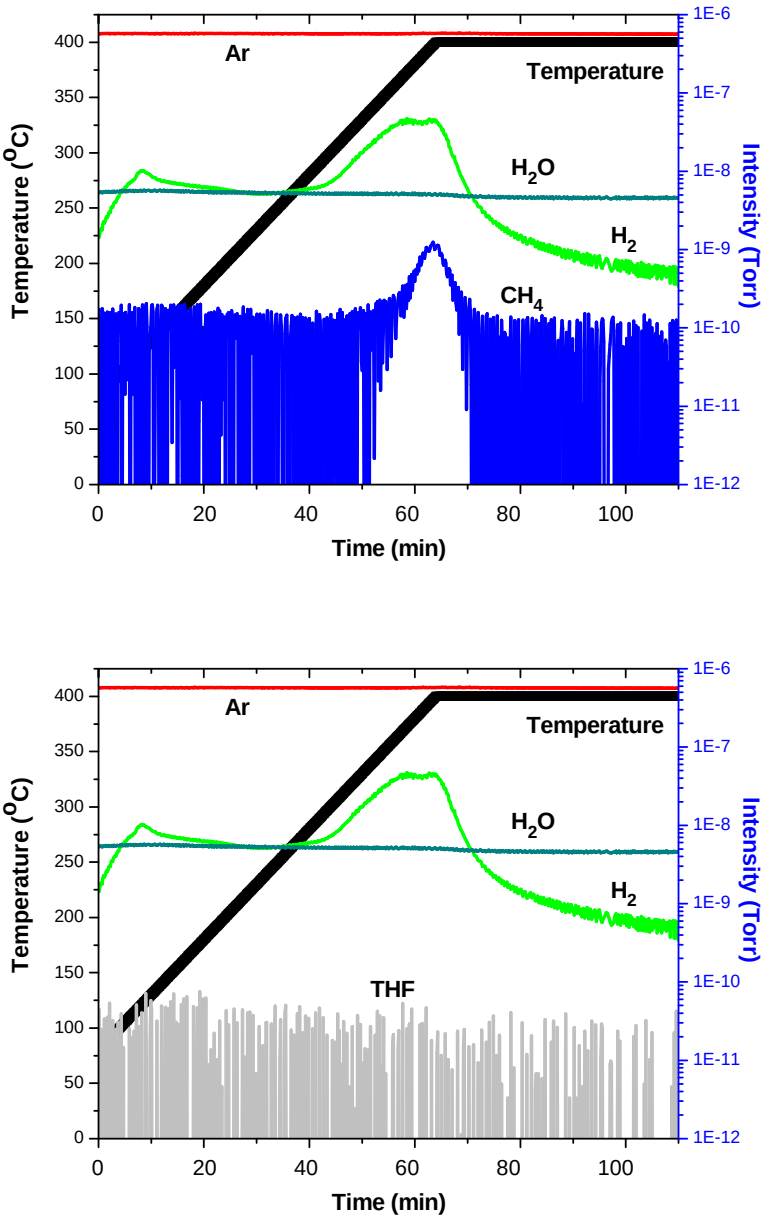

Figure 13. The composition prolife of the effluent gas from the TGA experiment of the nanoscale $LiBH_4$ infiltratated MgH_2 + 10 vol.% C mixture along with the temperature curve. Everything is the same for (a) and (b) except (a) highlighting the CH_4 profile and (b) focusing on the THF profile.

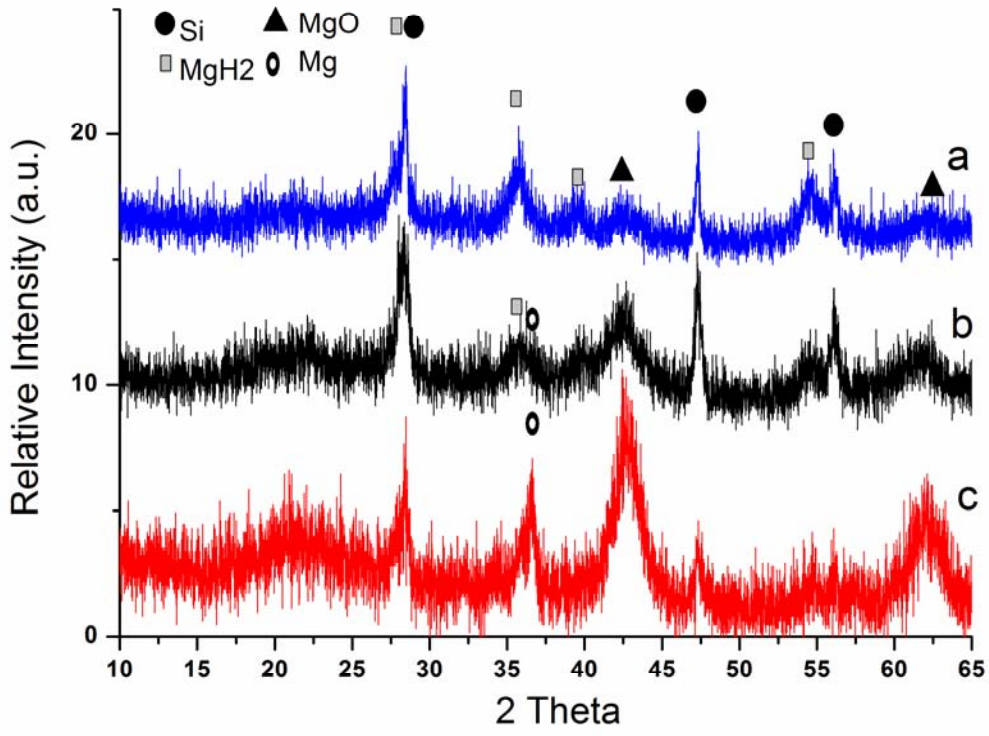

Figure 14. XRD patterns of (a) the nanoscale $LiBH_4$ infiltratated MgH_2 + 10 vol.% C mixture, (b) the sample (a) after dehydrogenation at 150°C, and (c) the sample (a) after dehydrogenation at 265°C. Note the presence of Mg in both samples (b) and (c), indicating that MgH_2 has decomposed to Mg and H_2 at both temperatures.